Statistical physics of earthquakes: Comparison of distribution exponents for source area and potential energy and the dynamic emergence of log-periodic energy quanta

JOURNAL OF GEOPHYSICAL RESEARCH, VOL. 105, NO. B3, PAGES 6105–6126, MARCH 10, 2000

Statistical physics of earthquakes: Comparison of distribution exponents for source area and potential energy and the dynamic emergence of log-periodic energy quanta

Ian G. Main

Department of Geology and Geophysics, University of Edinburgh, Edinburgh

Gareth O'Brien[1] and Jeremy R. Henderson[2]

Department of Geological Sciences, University of Durham, Durham, England

Abstract. We investigate the relationship between the size distribution of earthquake rupture area and the underlying elastic potential energy distribution in a cellular automaton model for earthquake dynamics. The frequency-rupture area distribution has the form $n(S) \sim S^{\tau} \exp(-S/S_0)$ and the system potential energy distribution from the elastic Hamiltonian has the form $n(E) \sim E^{\nu} \exp(-E/\theta)$, both gamma distributions. Here $n(S)$ reduces to the Gutenberg-Richter frequency-magnitude law, with slope $b \sim \tau$, in the limit that the correlation length ξ, related to the characteristic source size S_0, tends to infinity. The form of the energy distribution is consistent with a statistical mechanical model with l degrees of freedom, where $\nu=(l-2)/2$ and θ is proportional to the mean energy per site $\overline{E}$. We examine the effect of the local energy conservation factor β and the degree of material heterogeneity (quenched disorder) on the distribution parameters, which vary systematically with the controlling variables. The inferred correlation length increases systematically with increasing material homogeneity and with increasing β. The thermal parameter θ varies systematically between the leaf springs and the connecting springs, and is proportional to $\overline{E}$ as predicted. For heterogeneous faults, $\tau \sim 1$ stays relatively constant, consistent with field observation, and S_0 increases with increasing β or decreasing heterogeneity. In contrast, smooth faults produce a systematic decrease in τ with respect to β and S_0 remains relatively constant. For high β approximately log-periodic quanta emerge spontaneously from the dynamics in the form of modulations on the energy distribution. The output energy for both types of fault shows a transition from strongly quasi-periodic temporal fluctuations for strong dissipation, to more chaotic fluctuations for more conservative models. Only strongly heterogeneous faults show the small fluctuations in energy strictly required by models of self-organized criticality.

1. Introduction

The statistical properties of earthquakes in space, size, and time are of crucial importance in seismic hazard estimation. However, seismicity has only been recorded over a time period which is small compared to the typical average recurrence times of the largest earthquakes which dominate both the total seismic moment release and the damage. The earthquake frequency-magnitude distribution for such rare, damaging earthquakes can be constrained to some extent by the local seismic moment release rate, increasingly available at higher resolution from geodetic data from ground-based and satellite geodesy [*Kagan*, 1991, 1997; *Main*, 1996]. However, the moment release rate itself does not specify the type of distribution, only the parameters for a given distribution. This has given new impetus to the theoretical study of the form of the frequency-magnitude distribution for the rare, large events which dominate the seismic hazard.

One of the main lines of attack on this problem is the development of numerical models for earthquakes which reproduce the observed scaling properties [*Bak and Tang*, 1989; *Carlson and Langer*, 1989; *Ito and Matsuzaki*, 1990]. The scaling properties of such complex, nonlinear systems are "emergent" in the sense that they cannot be predicted linearly from the local physical interactions. Instead, they result from fundamental probabilistic and statistical mechanical constraints based on the cooperative response of the system for a large number of connected elements. One of the properties of this class of discrete numerical models, consistent with analytical theories discussed in section 2, is the emergence and maintenance of broad-bandwidth scale invariance in space and time [*Turcotte*, 1992; *Main*, 1996]. This property emerges as a consequence of spatial and temporal fluctuations in the local strain energy due to local threshold dynamics (brittle-field fracture or dynamic friction) in response to a constant external forcing from plate tectonics. In contrast to the temporal and geometrical properties of seismicity the underlying fluctuations in strain energy cannot be observed directly, although they can be

[1] Now at University College Dublin, Dublin.
[2] Now at Elf Exploration UK Public Limited Company, Aberdeen, Scotland.

Paper number 1999JB900396.
0148-0227/00/1999JB900396$09.00

determined in a straightforward way from numerical models [e.g., *Rundle et al.*, 1995, 1997a, b; *Schmittbuhl et al.*, 1996].

The aim of this paper is to examine the connection between the underlying distribution of strain energy and the resulting distribution of source rupture area in a numerical model for seismicity. We use the two-dimensional cellular automaton version of the conceptual *Burridge-Knopoff* [1967] spring-block-slider model proposed by *Bak and Tang* [1989]. Although the model is numerical, we fit the output data to analytical distributions, from percolation theory and statistical physics analogues, whose functional forms are found to be robust. We also examine temporal fluctuations in the mean energy $\bar{E}$ for the system as a whole. Following *Olami et al.* [1992], we examine the effect of the degree of local energy conservation as an important controlling variable and also the effect of varying degrees of material (strength) heterogeneity, or "quenched" disorder, in the system. We find that these parameters control the nature and magnitude of the energy fluctuations, as well as the parameters of the distributions of energy and source area, but do not control the form of the distributions themselves. We also find that the parameters for the local energy field and the distribution of source rupture area are correlated. First, we review the background theory and observation, discussing the advantages and disadvantages of the approach used.

2. Theoretical Background

2.1 Earthquake Statistics

At low magnitudes the frequency-magnitude relation takes the Gutenberg-Richter form:

$$\log n = a - bm \quad m \le m_{max}, \tag{1}$$

where n is the frequency of occurrence of a magnitude m in a time period T, a and b are the distribution parameters, and m_{max} is the maximum magnitude necessary to preserve a finite deformation (moment release) rate. Although (1) is commonly fitted to cumulative frequency data $N_C(x \ge m)$ to improve the smoothness of the line fit to the data, most of the underlying theories for the size distribution are formed in terms of incremental or discrete frequencies $n(m)$. Here we use the latter when we refer to "frequency".

For the usual case of seismic moment M scaling with source area S via $M \sim S^{3/2}$ and seismometers acting as velocity transducers, the Gutenberg-Richter law reduces to a power law for source area:

$$n(S) \sim S^{-b}, \tag{2}$$

with $b \sim 1$ [e.g. *Turcotte*, 1992]. Other forms of scaling of moment and magnitude give the same power law behavior but with a different slope b [e.g., *Romanowicz*, 1992; *Scholz*, 1994]. Equation (2) is only one example of broad-bandwidth scale invariance in the statistical priorities of earthquakes and faults [*Turcotte*, 1992; *Main*, 1996]. In section 2.2 we summarize some of the available theoretical models for the emergence of such scaling in complex systems.

2.2. Critical Points and Scaling

There are two main textbook models for the appearance of geometrical power law distributions such as (2), both of which have been developed to describe the behavior of two-phase systems near the critical point. Figure 1 shows an example of a phase change between a liquid and a gas in P-T (pressure-temperature) space. Below the critical point a change of phase occurs as a discrete jump in density which requires additional energy input in the form of latent heat. This is a first-order phase transition. The critical point (P_c, T_c) is defined as the point where the density difference between the two phases disappears, so that it is equally energetically favorable for either phase to exist. This is referred to as a "second order" phase transition.

The predominance of one phase over another is described by an 'order' parameter, which in this case can be defined as the difference in density between the liquid and gas phases. The order parameter is high when the liquid phase dominates, decreases rapidly toward the critical point, and is zero at and above the critical temperature. As the critical point is approached, the competition of local molecular interactions tending to produce order and thermal fluctuations tending to produce disorder increasingly balance, resulting in an order parameter which decreases nonlinearly to zero. At the same time the competition of local physical interactions and thermal fluctuations results in the development of scale-invariant clusters, associated with the emergence of long-range correlations in the model structure, confirmed by experiment on a wide variety of physical systems [e.g., *Bruce and Wallace*, 1989].

The type of phase transition illustrated on Figure 1 may occur in two ways: either from one state of order to another (liquid to gas) by decreasing the pressure at $T=T_c$ or by increasing the temperature at $P=P_c$, in which case this is known as an order-disorder phase transition, because random thermal fluctuations dominate above T_c. Thus the path in P-T space plays a large role in the nature of the spatial correlations that emerge. The behavior of critical point systems can be modeled using the techniques of statistical physics, based on a probabilistic description of the energy field resulting from local interactions [*Stanley*, 1971]. This approach combines local physics, geometry, and a stochastic thermal element. Alternatively, we may adopt a purely

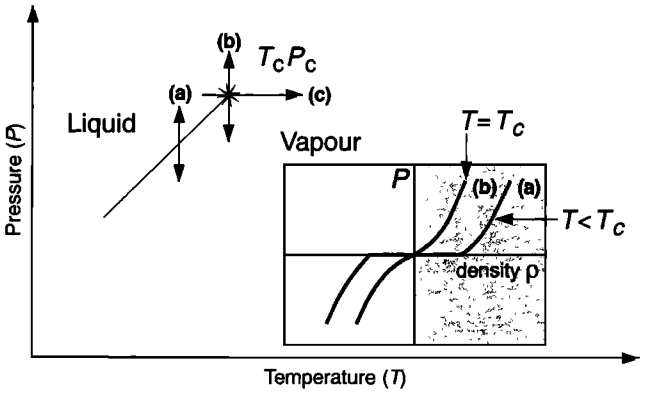

Figure 1. Phase diagram in P-T space for the transition between a liquid and a gas. The solid line represents the boundary between the two, which disappears at a critical temperature T_c and pressure P_c. At this point the density difference between the two phases disappears (see inset). A first-order phase transition at constant pressure is shown (labeled a). Two second-order phase transitions at the critical

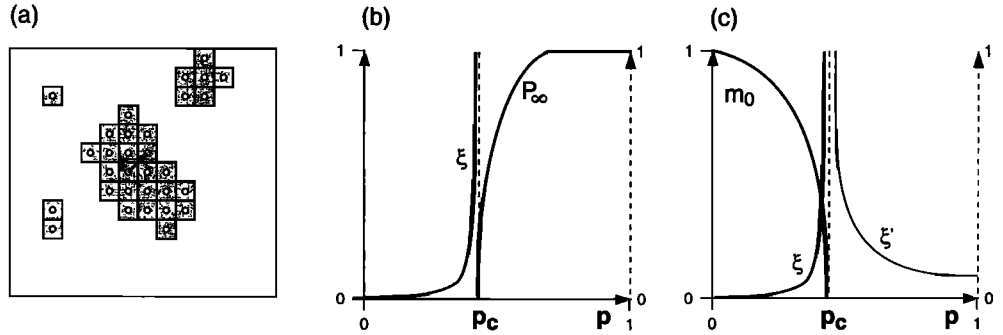

Figure 2. Schematic examples of phase transitions near the critical point. (a) Illustration of the site percolation problem. (b) A percolation model for the probability P_∞ of an individual cluster spanning the model space as the probability p of occupying an individual site increases [after *Stauffer and Aharony*, 1994]. Here p_c is the percolation threshold, where at least one cluster spans the model space and the correlation length ξ becomes infinite. This is an example of an order-order transition at the critical point, corresponding to the path b shown in Figure 1. (c) Schematic results from Ising model for the normalized spontaneous magnetization m_0 as the temperature T increases through the critical temperature T_c (here the Curie temperature) [after *Bruce and Wallace*, 1989]. In this case the order parameter m_0 is identically zero above the critical temperature, representing an order-disorder phase transition similar to path c in Figure 1. In this case the correlation length is finite both above and below the critical point.

statistical approach, for example, applying percolation theory [*Stauffer and Aharony*, 1994]. A brief description of the main generic results of both approaches follows.

2.3. Percolation Theory

Percolation theory can be applied to a range of phenomena involving the clustering properties of a binary system. The summary here is taken from *Stauffer and Aharony* [1994, chapter 2], which also deals with the two-phase system of "empty" or "occupied" sites illustrated in Figure 2a. The main difference with their nomenclature is that we use n to refer to the frequency of cluster size rather than the probability of a single cluster element belonging to a cluster of size S. The results can be compared to those of *Stauffer and Aharony* [1994] by replacing our n with their n divided by S. In a percolation problem, elements in a d-dimensional system are filled at random with an increasing probability p, so that a variety of different geometrical forms of connected clusters of filled elements may result. In two dimensions the size-frequency distribution of the connected clusters takes the form

$$n(S) \sim S^{-\tau} e^{-cS}, \tag{3}$$

where $S_0=1/c$ is a characteristic dimension related to the correlation length ξ, defined by

$$\xi^2=\Sigma_r [r^2 g(r)] / \Sigma_r [g(r)], \tag{4}$$

where $g(r)$ is the correlation function, that is, the probability that a site at distance r from an occupied site is also occupied and belongs to the same cluster. This can also be written as

$$\xi^2=\Sigma_s [R_S^2 S^2 n(S)] / \Sigma_r [n(S)], \tag{5}$$

where, for a given size of clusters S, R_S is the radius of gyration and $2R_S^2$ is the averaged squared distance between two connected cluster sites. The radius of gyration depends on the roughness of the connected cluster, quantified by its fractal dimension D via

$$R_S \propto S^{1/D}. \tag{6}$$

As the probability p increases, eventually there is a finite probability that a single cluster spans the model space. This point is known as the percolation threshold p_c. The correlation length diverges as $p \rightarrow p_c$ according to

$$\begin{aligned} \xi &\propto |p-p_c|^{-\nu} & \xi < p_c \\ \xi &= \infty & \xi \geq p_c, \end{aligned} \tag{7}$$

while

$$c \propto |p-p_c|^{1/\sigma}, \tag{8}$$

where ν and σ are critical exponents of the system. From (3)-(8) we can show that $D=1/\sigma\nu$. D is 1.896 for $d=2$, and $D=2.5$ for $d=3$.

If P_∞ is the fraction of lattice sites belonging to a network connected to at least two opposite edges (the infinite network), then

$$\begin{aligned} P_\infty &\propto c^{\tau-2} \propto |p-p_c|^{B} & p > p_c \\ P_\infty &= 0 & p \leq p_c, \end{aligned} \tag{9}$$

where the critical exponent $B=(\tau-2)/\sigma$. Thus the probability of the infinite cluster increases smoothly as a power law as p increases above p_c (schematically shown in Figure 2b). In contrast, the correlation length diverges as $p \rightarrow p_c$. P_∞ is another example of an "order" parameter, in the sense that it measures the probability of neighboring sites having the same property of being both occupied and connected to the edges of the model space. Percolation actually describes a transition from one ordered state (all sites unoccupied at $p=0$) to another ordered state (all sites occupied at $p=1$). On

Figure 1 this is analogous to a phase transition at constant temperature T_c, where all elements belong initially to the same phase (unoccupied sites) at p=0 and to the second phase (occupied sites) at p=1. Thus the statistical mechanical model is the more general, although both are identical precisely at the critical point.

2.4. Statistical Mechanics

The basis of statistical mechanics is the distribution of the local energy in a system of many discrete elements [e.g., *Mandl*, 1988]. The Hamiltonian is defined as the sum of the local potential and kinetic energies, although in calculating the scaling properties the kinetic energy terms are often neglected. For example, the Hamiltonian for a ferromagnet takes the following form:

$$H = -\Sigma_{i=1,N} \Sigma_{j=1,N} J_{i,j} \boldsymbol{S}_i \bullet \boldsymbol{S}_j - \mu\Sigma_{i=1,N} \boldsymbol{S}_i \bullet \boldsymbol{H}, \qquad (10)$$

where J is the spin exchange force, which tends to align the magnetic spin vectors $\boldsymbol{S}_i$ and $\boldsymbol{S}_j$ at two different positions i and j, and decays strongly with distance; $\boldsymbol{H}$ is the external magnetic field; μ is the constant of proportionality between the magnetic moment vector $\boldsymbol{m}$ and the spin vector $\boldsymbol{S}$; and N is the number of elements in the system. The first term on the right hand side combines the effect of local interactions and fluctuations, and the second term introduces the effect of the external field $\boldsymbol{H}$. The Hamiltonian formulation allows the tendency of neighboring fields to align to increase the spontaneous magnetization (decreasing H) to be opposed by thermal fluctuations, which lead to increasing H. The Hamiltonian is related to the mean energy per site $\overline{E} = \langle H \rangle / N$, where N is the total number of sites in the model. Thermal fluctuations introduce a degree of disorder into the system and hence a reduction in the spontaneous magnetization $m_{H=0}$, denoted m_0 below, which serves as an appropriate order parameter for the system. As temperature increases, the tendency of neighboring fields to align to increase m_0 is opposed by thermal fluctuations which contribute increasingly to the mean energy. This induces a degree of disorder into the system and a reduction in m_0. Again, it is the competition between local interactions and thermal fluctuations which leads to long-range correlations in the model [e.g., *Bruce and Wallace*, 1989].

The complete problem is often simplified in numerical models for magnetization as follows. First, the model is made computationally tractable by coarse graining, that is, making the model elements much larger than the atomic size of a discrete elemental spin. This can be justified near the critical point, based on analytical renormalization group rescaling models which accurately predict the relevant critical exponents as the model is rescaled to different sizes [*Stauffer and Aharony*, 1994]. Second, knowing that the spin exchange force decays rapidly with distance, it is common to consider only nearest-neighbor interactions. Third, the problem is often reduced to a binary system by allowing spins to be either parallel or antiparallel to the external field. This set of assumptions is used to produce the "Ising" model for magnetization. Finally, the models are often calculated for d=2. These sets of assumptions are known to be at worst incorrect and at best approximate, but nevertheless, they lead to a model for magnetization which adequately predicts the observed nonlinear decrease in m_0 to zero as $T \rightarrow T_c$. In fact, the strongest control on the critical exponents measuring this decay is the dimensionality of the model, so that an exact match to the observed critical exponents can only be obtained with d=3 [*Stanley*, 1971]. The reason the distributions, if not the precise value of their critical exponents, are relatively insensitive to the simplifying assumptions is that the global properties are constrained by fundamental statistical mechanical and geometrical constraints which dominate the behavior [*Stanley*, 1971].

From maximum entropy arguments [e.g., *Mandl*, 1988] the distribution of local energy in statistical mechanics commonly takes the form of a Boltzmann exponential:

$$n(E) \sim g_E e^{-E/\theta}, \qquad (11)$$

where $\theta = k_B T$, k_B is Boltzmann's constant, and the factor g_E represents the number of ways a particular energy level can be attained. Here g_E may be a constant, in which case the classic Boltzmann exponential distribution is recovered, or it may vary systematically with energy. The mean energy is then the first moment of this distribution:

$$\overline{E} = \Sigma_{i=1,N} E\, n(E) / \Sigma_{i=1,N}\, n(E), \qquad (12)$$

where again N is the total number of elements. For g_E=1, (12) reduces to $\overline{E} = \theta = k_B T$. The denominator in (12) is known as the "partition function" of statistical mechanics:

$$Z = \Sigma_{i=1,N}\, n(E). \qquad (13)$$

The partition function is related to the Helmholtz free energy F by $F = -k_B T \ln Z$. In this way, Z can be used to calculate thermodynamic variables on a larger scale. For the Ising model both the analytical model (in the limit of large N) and the coarse-grained numerical equivalent predict scaling relations of the form:

$$\begin{aligned} m_0 &\propto (T_c - T)^B \quad && T < T_c \\ m_0 &= 0 && T \geq T_c, \end{aligned} \qquad (14)$$

and

$$\begin{aligned} \xi &\propto |T_c - T|^{-\nu} && T < T_c \\ \xi' &\propto |T_c - T|^{-\nu'} && T \geq T_c, \end{aligned} \qquad (15)$$

where for d=2, it can be shown that B=1/8 and ν=ν'=1. This result is shown schematically in Figure 2c [after *Bruce and Wallace*, 1989]. Equation (14) for the order parameter m_0 has the equivalent form to (9) (except that the x axis is reversed, compare Figures 2b and 2c). Equation (15) for the correlation length has the equivalent form to (7) (except that the correlation length is finite above the critical point for an order-disorder transition). This illustrates the fundamental similarity of the percolation threshold and the critical point [*Stauffer and Aharony*, 1994], although we note that the relevant exponents need not be the same, because of the presence of interactions in the physical model.

2.5. Self-organized Criticality

The systems described in section 2.4 are assumed to be in thermodynamic equilibrium. This is not appropriate for modeling populations of earthquakes or faults, which are driven very far from equilibrium by a continuous input of strain energy from the steady motion of Earth's lithosphere.

Such systems are fundamentally irreversible and dissipative and involve an energy flux which acts to vary $\overline{E}$ in time, but which also acts to push the system toward criticality. In contrast, the threshold nature of earthquake mechanics, leading to a local stress relaxation during rupture, tends to move the system away from criticality. The dynamic balance of the two may maintain the system in a perpetual state of near criticality, without the need for the external tuning of the external variables that would be necessary for other types of phase transition. Such systems, maintained spontaneously at or near the critical point, are said, instead, to be in a state of "self-organized criticality" [*Bak et al.*, 1987], a paradigm which in its broad sense has been applied very successfully to the explanation of many of the scaling rules observed in seismology, notably the form of (1) [*Bak and Tang*, 1989; *Sornette and Sornette*, 1989; *Ito and Matsuzaki*, 1990].

Despite its name some external tuning is often necessary in practice to match the observed scaling exponents in numerical models. For example, the cellular automaton model of *Olami et al.* [1992] showed that the quantitative observation $b \sim 1$ can only be attained for a particular amount of local energy dissipation. In the solid Earth, there is no external agent to affect this tuning. The threshold nature of the locally brittle mechanics involved also introduces a conceptual problem in the application of critical point phenomena to the interpretation of the results. For the problem of tensile fracture with a finite opening displacement it is relatively easy to imagine a two-phase system of intact or broken elements, forming the rock matrix and porosity, respectively. In contrast, it is hard to imagine a direct analogue for the second phase in earthquake problems, since the fault rupture heals effectively instantaneously compared to the geological timescales of the external forcing. The second phase of broken elements exists only fleetingly during earthquake rupture, having a short duration compared to the discrete timestep of a numerical model. Nevertheless, it is treated statistically similarly to the fracture problem as a second phase with a finite lifetime.

The idea of using the frequency-magnitude diagram to identify likely positions in the phase diagram near the critical point was first suggested by *Lomnitz-Adler* [1993], who reviewed a host of different quasi-static cellular automaton models for seismic fracture and identified three generic types of distribution universal to all the models reviewed. *Mousseau* [1996] extended this principle and derived a phase diagram for earthquake recurrence using the quasi-static model of *Olami et al.* [1992]. He used the degree of force dissipation and the degree of quenched disorder (material heterogeneity) to define four separate "phases", based on similarities in the form of the cluster size distribution and the synchronicity of seismic events in the model. The results demonstrate that the variable degree of energy dissipation and the level of quenched disorder (material heterogeneity) in the model both exert a strong control on the distribution parameters and on the location of the phase boundaries. Using the same model, *Ceva* [1995] showed that the nature of quenched disorder can have a strong effect on the observed behavior, with point defects having more impact than more extended heterogeneities. *Dahmen et al.* [1998] examined the behavior of a three-dimensional dynamic earthquake model including inertial terms, and calculated the position of the phase boundary between a "small earthquake" phase with a finite correlation length and a "metastable" phase with large characteristic earthquakes, depending on the values of the characteristic cut off size and the slip-weakening amplitude. Their model predicts a first-order phase transition between the two phases, in the sense that there is a finite gap between the size of the largest events and the rest of the population. (For a second-order phase transition the distribution of cluster sizes is continuous).

Numerical models for faulting and earthquakes often simplify the local physics to an unrealistic degree. For example, constitutive mechanical rules are used which are known to be much simpler than those implied by the observation of rate and state dependence of frictional slip in laboratory sliding experiments [*Deiterich*, 1979]. However, we have seen that the scaling properties of other near-critical systems are robust with respect to the details of the assumed local dynamics. Another inherent drawback of such models is that they are inherently "coarse-grained", in the sense that their discrete elements have a spatial dimension which is much larger than both the grain size of the material and the critical slip distance implied by the rate and state frictional law [*Rice*, 1993]. Again, we have also seen that coarse graining does not strongly affect the generic observations of the scaling relations listed above. The models used are often only one- or two-dimensional, so that true three-dimensional effects are often neglected including any coupling to a more ductile substrate in the lithosphere [*Ben-Zion et al.*, 1993]. We have seen above that the dimensionality strongly affects the particular critical exponents, if not the generic form of the behavior near the critical point.

The strongest argument in favor of earthquakes as self-organized critical (or near critical) point phenomena remains their spectacular success in explaining the temporal and spatial scaling properties of seismicity and faulting [*Turcotte*, 1992; *Main*, 1996]. This implies not only that the scaling properties of seismicity and faulting are fairly robust, despite the drawbacks acknowledged above, but also that their generic forms, if not their precise exponents, are relatively insensitive to the details of the local dynamics involved. In this paper we concentrate on examining the scaling properties of the distribution of local energy and rupture area. We find that the generic forms are retained for a wide variety of model parameters but that the parameters of the distribution are sensitive in a systematic way to the model heterogeneity and the local energy dissipation.

2.6. Energy Distributions

The output of numerical models includes full knowledge not only of the frequency-area statistics for individual ruptures but also of the underlying energy distributions which give rise to them. In recent years the distribution of local potential strain energy has been examined by a number of authors for a variety of numerical models of earthquakes as critical or near-critical point phenomena [*Rundle et al.*, 1995, 1997a, b; *Schmittbuhl et al.*, 1996]. This allows examination of spatiotemporal fluctuations in the local energy associated with the buildup and release of tectonic strain energy and hence the effect of nonequilibrium properties on the dynamics. The generic form of the energy distribution in such numerical models [e.g., *Rundle et al.*, 1995] takes the form

$$n(E) \sim E^{\eta} e^{-E/\Theta}, \tag{16}$$

implying $g_E \sim E^{\gamma}$. This result can be predicted from assuming the energy distribution to result from a reduced chi-square distribution with l degrees of freedom:

$$\gamma = (l-2)/2. \quad (17)$$

Thus the distribution of rupture area (3) and local energy (16) both take the form of a gamma distribution, that is, a power law for low S or E, and a decreasing exponential at higher values. The change in behavior occurs at a size determined by the correlation length and the mean energy. In this paper we address the utility of (3) and (16) for describing the statistical properties of earthquakes from a spring-block-slider model and examine the possibility of a correlation in the distribution parameters.

3. Model Description

The numerical model used here is based on the *Burridge-Knopoff* [1967] spring-block-slider model of earthquake rupture, as applied to earthquake dynamics by *Bak and Tang* [1989], referred to here as the BT model, and by *Olami, Feder and Christensen* [1992], hereafter referred to as the OFC model. Our model is similar to the BT model, except that we include a variable dissipation rule in the spirit of the OFC model, with the important caveat that the effects of the connecting springs between neighboring elements and the leaf springs connected to the driving plate are examined separately. We use a two-dimensional version of the BT model in which a driving plate is maintained at a constant velocity V, continuously adding strain to $N=N_i \times N_j=128\times128$ fault elements (blocks) of dimension Δx via a leaf spring of stiffness k_L. The seismic moment release rate is then

$$dM/dt = k_L N_i N_j \Delta x^2 V = k_L WLV, \quad (18)$$

where L is the macroscopic fault length and W is its width. The individual blocks interact via connecting springs with stiffness k_C. A rigorous application of elasticity theory to the Burridge-Knopoff model is provided by *Leung et al.* [1997]. However, owing to this analytical complexity, simpler forms are usually applied in numerical models. For example, the Hamiltonian for the OFC model, again neglecting the kinetic energy terms, is

$$H = (k_C/2)\,\Sigma_{i=1,N}\Sigma_{j=1,N}\,\delta(|r_i-r_j| - \Delta x)(u_i-u_j)^2 + (k_L/2)\,\Sigma_{i=1,N}(Vt-u_i)^2, \quad (19)$$

where u_i is the displacement and r_i is the position vector at the ith element. Here δ is Kronecker's delta, so that only nearest neighbors are considered in the interactions. This result follows from assuming that k_C and k_L are spatially homogeneous, so they can be brought outside the summation terms. The first term on the right-hand side of (19) represents the internal fluctuations and interactions, and the second term represents the effect of the external field.

There are four connecting springs but only one leaf spring per element, implying that the statistical properties of the leaf springs and the internal springs may be different (l=4 and 1, respectively). Therefore we examine the effect of both separately. For the BT model the Hamiltonian is approximated by

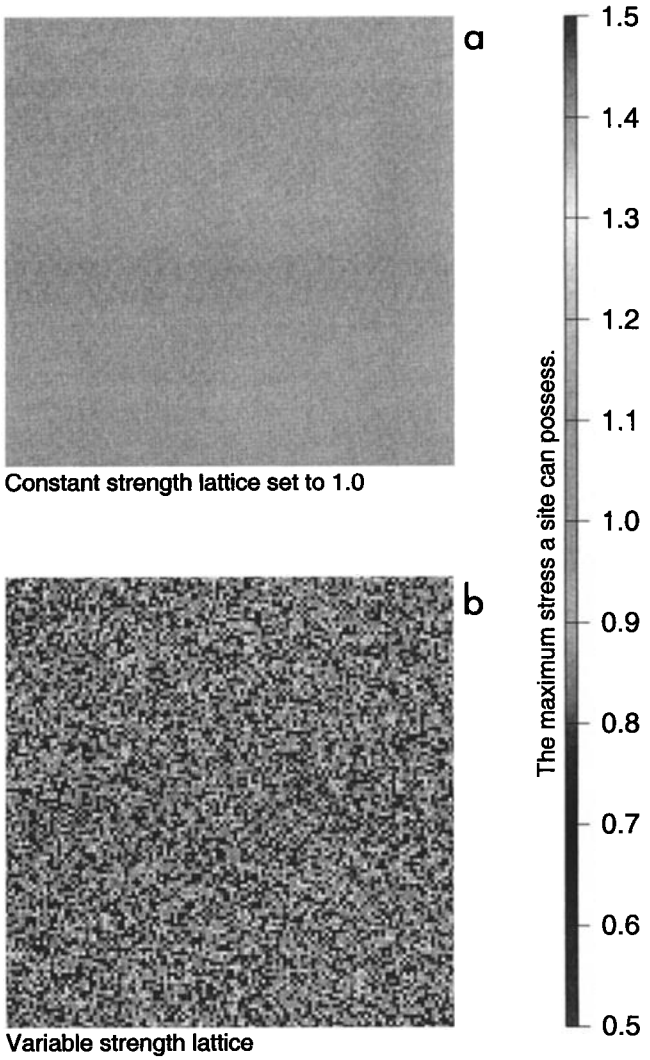

Figure 3. Plot of the material heterogeneity for the two generic models for (a) a smooth fault (constant strength $\sigma_F^{i,j}=1$) and (b) a rough fault, with a random spatial distribution of strengths between 0.5 and 1.5 dimensionless units and a mean strength $\langle\sigma_F^{i,j}\rangle=1$.

$$H = (2k_C)^{-1}\,\Sigma_{i=1,N}\Sigma_{j=1,N}\,\delta(|r_i-r_j| - \Delta x)(F_i-F_j)^2 + (2k_L)^{-1}\,\Sigma_{i=1,N}(F_i)^2. \quad (20)$$

At time t=0 we assign a local strength $\sigma_F^{i,j} = F_F^{i,j}/\Delta x^2$ to each element to be either uniform (equal to 1 in normalized units) or a random number between limits σ_F^{min} and σ_F^{max} (Figure 3). We refer below to the former as a homogeneous or "smooth" fault, and the latter as a heterogeneous or "rough" fault. This allows an examination of the influence of permanent strength heterogeneity (quenched disorder) on the results in a manner similar to that applied by *Janosi and Keresz* [1993], *Ceva* [1995] and *Mousseau* [1996]. We assume the leaf springs are much stiffer than the connecting springs ($k_L=30k_C$).

We define a discrete time step $\Delta t=\Delta\sigma/\langle\sigma_F\rangle=1/200$ and add an amount of stress, $\Delta\sigma+\eta(x,t)$, to each element from the action of the leaf springs. Here $\eta(x,t)$ is a random number which accounts for disorder introduced by random local fluctuations in space and time, playing the same role as thermal fluctuations in the examples given above. In nature

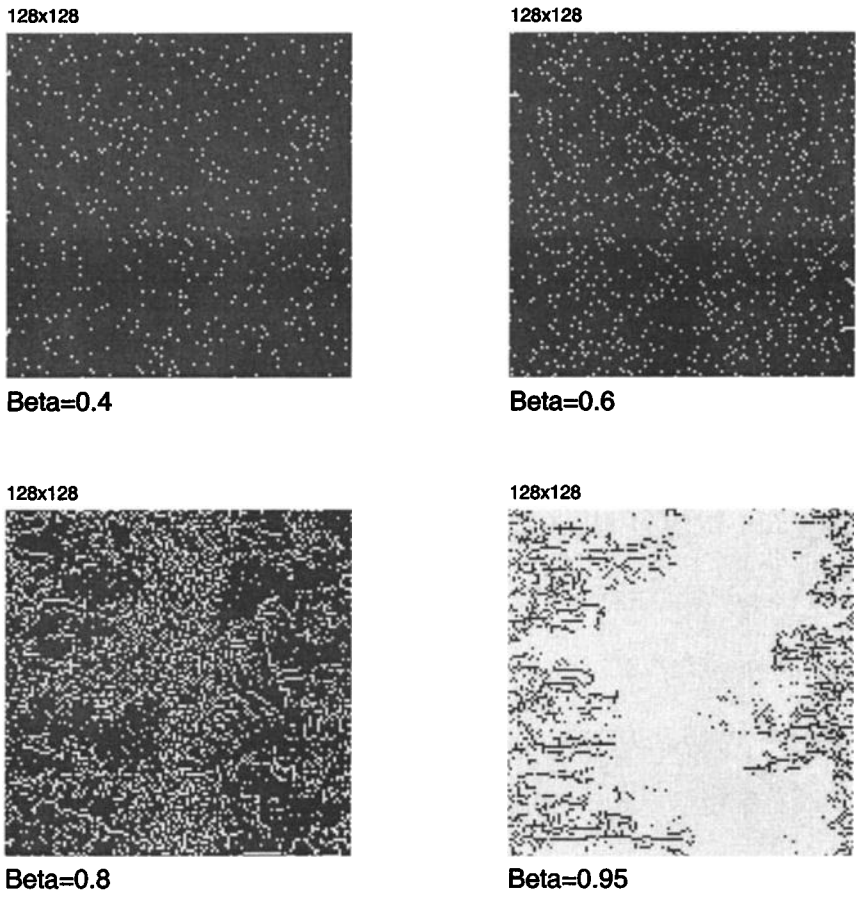

Figure 4. Plot of the distribution of failed elements in a single time step for different values of the conservation parameter β. The connected areas in white indicate individual ruptures during that particular time step.

such fluctuations are not due to variations in temperature, which would be relatively constant within a block of such large dimensions but result from fluctuations in the stress field brought about by dynamic interactions [e.g., *Carlson and Langer*, 1989] or effects not explicitly considered here, such as local pore pressure.

If the local stress exceeds the failure stress, $\sigma^{i,j} \geq \sigma_F^{i,j}$, the element is deemed to have failed, and we distribute the relaxed stress to the four nearest neighbors according to the following "jump rule":

$$\sigma^{i\pm1, j\pm1} = \beta \sigma^{i,j} / 4$$
$$\sigma^{i,j} = 0. \quad (21)$$

This differs from the BT model by the introduction of a factor β which determines the amount of dissipation of energy in the system at a local scale. In the OFC model, β is fixed by the ratio of spring stiffnesses, but here we assume β is a free parameter. Thus the stress is relaxed totally at the broken element and transferred with some dissipation to the nearest neighbors. If the nearest neighbor also fails, then the rupture proceeds in a cascade of connected N_F failed elements with rupture area $S=N_F\Delta x^2$. If an element fails, we assume it cannot sustain any additional stress during an individual rupture propagation. This results in an additional source of stress dissipation during implementation of the jump rule. During rupture we treat the model boundaries as absorbing, so that stress is also relaxed at the edges of the model space. Once rupture stops, we assume an immediate healing of an element to its former strength.

4. Results

4.1. Smooth Fault

4.1.1. Statistical properties. The distribution and morphology of model ruptures, taken at an arbitrary time step for illustration purposes, is shown for the case of a smooth fault in Figure 4 for different values of β. Note that the size of the largest clusters increases systematically as β is increased, implying an increase in the correlation length. The snapshot for β=0.95 shows a single percolating cluster. Figure 5 shows the frequency-area statistics for the connected clusters, determined from a sequence of snapshots such as Figure 4, averaged over the whole model run (4000 time steps). The results show good agreement with (3), which was fitted to the data using a least squares fit by standard least squares regression for

$$n_S = C S^{-\tau} e^{-\alpha S}, \quad (22)$$

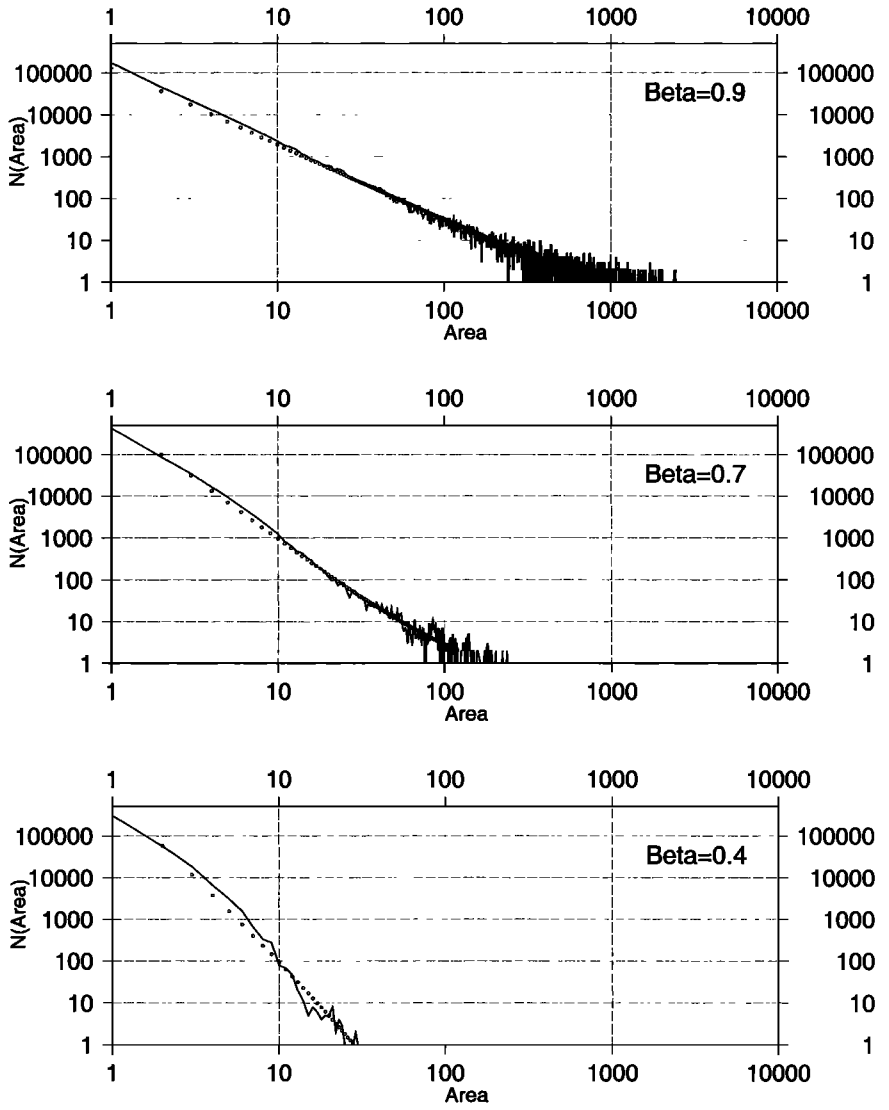

Figure 5. Frequency-area statistics of the model ruptures, summed over an entire model run for different values of β. The circles represent best fits to equation (22) using (23).

by solving the matrix equation:

$$\begin{pmatrix} ln\,[n(S_1)] \\ \dots \\ ln\,[n(S_N)] \end{pmatrix} = \begin{pmatrix} 1 & ln\,[S_1] & S_1 \\ \dots & \dots & \dots \\ 1 & ln\,[S_N] & S_N \end{pmatrix} \times \begin{pmatrix} ln[C] \\ \tau \\ c \end{pmatrix}. \quad (23)$$

The results for the best fitting parameters are listed in Table 1. Note that for the case of a smooth fault it is possible to have near-zero or negative values for the exponent c for high conservation factors. These models correspond to the case of a correlation length which is comparable in size with the dimensions of the model, analogous to the "characteristic" earthquake model or the crossover phenomenon in percolation theory [e.g., Figure 16 of *Stauffer and Aharony*, 1994]. The transition from below to above the percolation threshold occurs for β≈0.8.

A typical snapshot for the energy distribution in the leaf springs on the lattice is shown, also for the case of a smooth fault, in Figure 6. This distribution is continuous in energy, in contrast to the binary field of the rupture distributions shown in Figure 4. The resulting energy field is largely uncorrelated for a high degree of dissipation but becomes increasingly correlated for low dissipation. For example, the snapshot for β=0.95 in Figure 6 shows a percolating cluster for normalized energies, as a proportion of the maximum energy, in the range 0.4-0.6 (mid-grey tone). Note also the stress concentrations at the boundaries of this object (slightly darker grey tone). The long-range correlations formed by the percolating cluster are related to peaks in the energy distribution shown in Figure 7. These peaks take the form of discrete quanta superposed on the underlying Boltzmann trend of (16). The quanta and the associated spatial correlations in energy level both disappear with increasing dissipation and are largely absent below the percolation

Table 1. List of Model Input Parameters (Strength Range and Conservation Factor β) and Output Parameters

Strength Range	β	τ	c	γ	1/θ	$\overline{E}$
1.0	0.9	1.83	-0.001	2.426	4.142	0.930
1.0	0.8	2.32	-0.003	2.430	4.416	0.866
1.0	0.7	2.96	0.011	2.431	4.760	0.800
1.0	0.6	3.56	0.025	2.310	5.230	0.725
1.0	0.4	3.87	0.026	2.400	6.600	0.595
0.5-1.5	1.0	1.03	0.001	2.70	3.142	1.58
0.5-1.5	0.9	1.25	0.029	2.58	3.432	1.36
0.5-1.5	0.8	1.18	0.084	2.08	3.320	1.18
0.5-1.5	0.7	1.60	0.116	2.03	3.655	1.05
0.5-1.5	0.6	0.99	0.482	2.13	4.355	0.94
0.5-1.5	0.4	0.96	0.535	1.83	5.012	0.73

threshold β<0.8 (Figures 6 and 7). This implies that they result from dynamic rather than purely geometric constraints.

The energy distribution for the connecting springs takes a different form. Examples, averaged over the model run, are shown in Figure 8. The model output compares well to the theoretical distribution

$$n_E = C_E E^{\gamma} e^{-E/\theta} \tag{24}$$

using the same algorithm used to solve (23). Figure 8 also plots the best fit lines to this distribution. The results are also summarized in Table 1. The exponent γ≈2.4 stays relatively constant in this case, with the temperature term θ increasing as the level of conservation increases. We note that the generic form of (24) is maintained, although the exponent γ is significantly higher than the value γ=1 predicted by (17) for a system with l=4 degrees of freedom. This implies that the

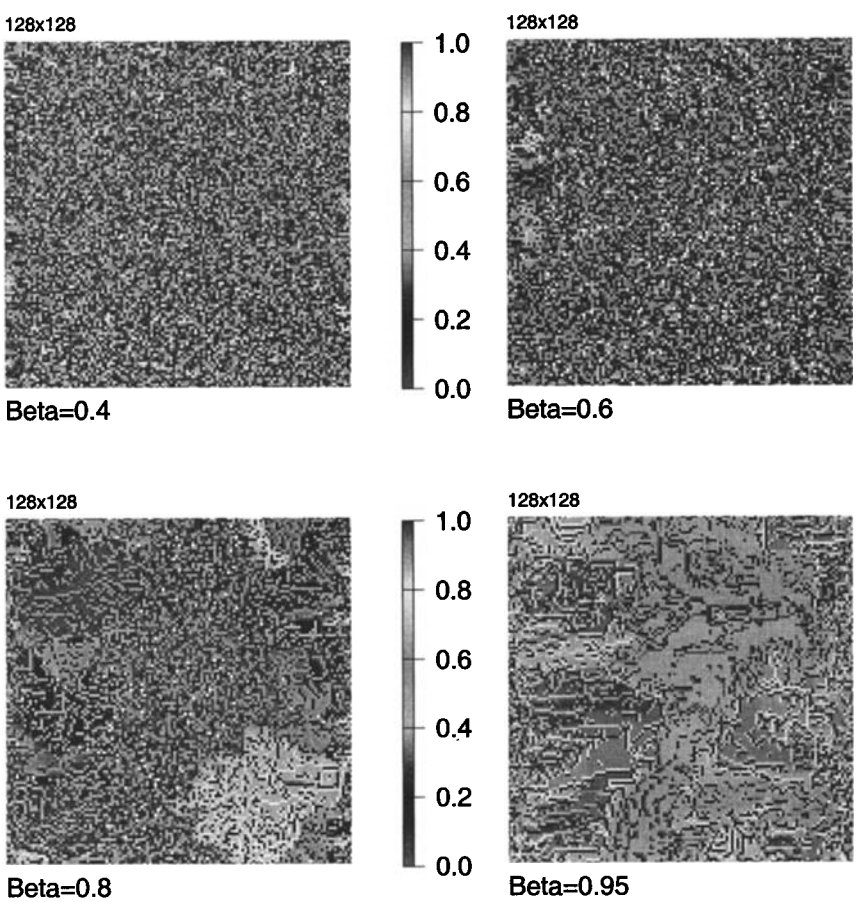

Figure 6. A snapshot of the energy distribution in the leaf springs as a function of the conservation parameter β. Note the emergence of long-range correlations as β is increased.

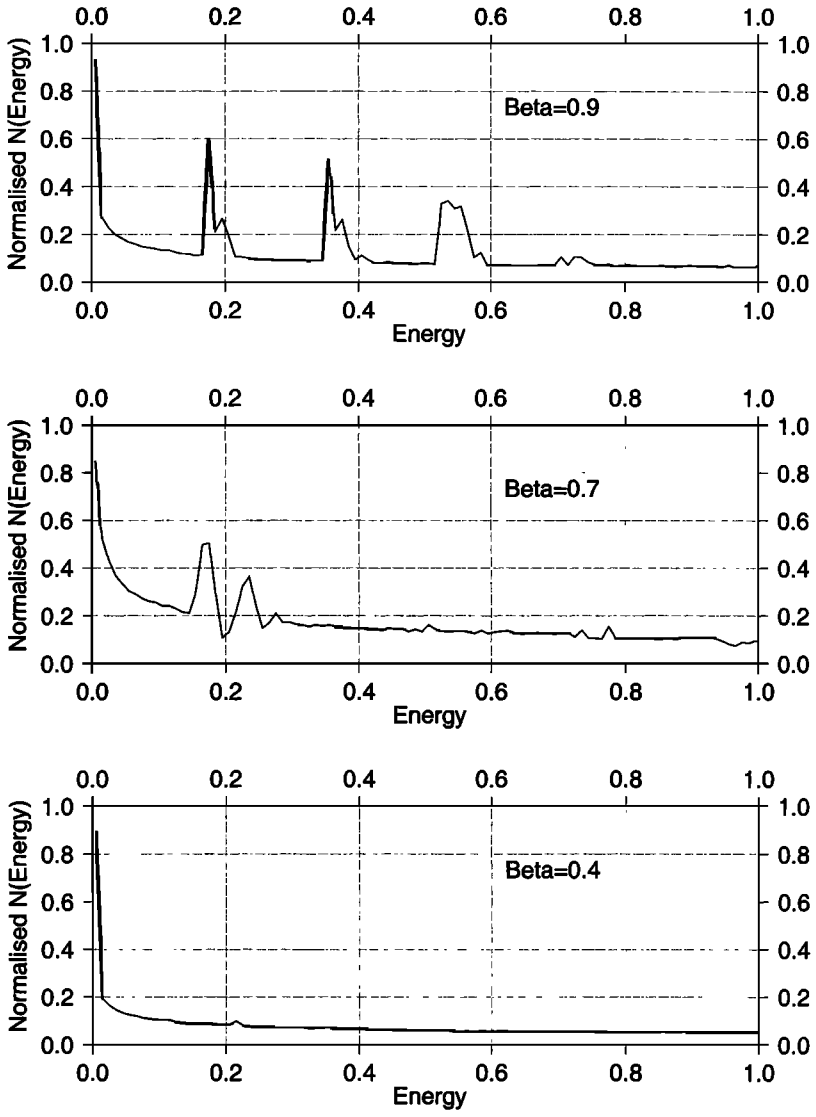

Figure 7. Plot of the energy distribution in the leaf springs, averaged over the model run for different β. Note the development of preferred energy states for high conservation due to emergent long-range correlations in the energy field.

simple chi-squared model may not be a precise quantitative model for the system of interest here. In fact, the noninteger values of l implied by the results in Table 1 suggest a fractal rather than an integer-based distribution. The physical origin of this observation has yet to be established. Nevertheless, the statistical properties, averaged over the model run, show a good agreement with the predictions of critical point phenomena described in section 2.

4.1.2. Energy fluctuations. One of the central questions to be addressed in earthquake dynamics is the degree of predictability of the emergent time series [*Main*, 1996]. In fact, models for earthquake dynamics can show a large range of behavior, from periodic to random, depending on the input variables and the model used [e.g., *Christensen*, 1992; *Grassberger*, 1994; *Sornette et al.*, 1994; *Middleton and Tang*, 1995]. In this section we examine the nature of the temporal fluctuations in mean energy $\overline{E}(t)$ as a function of β, shown in Figure 9. For low values of β the system exhibits quasi-periodic fluctuations in $\overline{E}$ after an initial settling-in period. The emergence of quasi-periodic fluctuations for low conservation is also a property of the model of *Janosi and Keresz* [1993] for sandpile dymanics. The model above is set up with a dimensionless characteristic time t_C=200 for a smooth fault with no local fluctuations, $\sigma_F^{i,j}$=1 and $\eta(r,t)$=0. In fact, the periodicity in $\overline{E}(t)$ for β=0.4 shows 33 cycles in 4000 time steps or a typical period of t_R=121 time steps for finite $\eta(r,t)$. This reduction in mean recurrence time of the large events occurs as a consequence of internal energy being added to the system by the local fluctuations. As β is increased, the periodicity disappears, and the temporal fluctuations in mean energy become more chaotic, also as seen in the model of *Janosi and Kertesz* [1993]. For intermediate β the spectrum of $\overline{E}(t)$ shows a mixture of the two, with a characteristic peak indicating periodicity superposed on a trend which decays with frequency broadly according to $1/f$ noise (Figure 10). Two other systematic

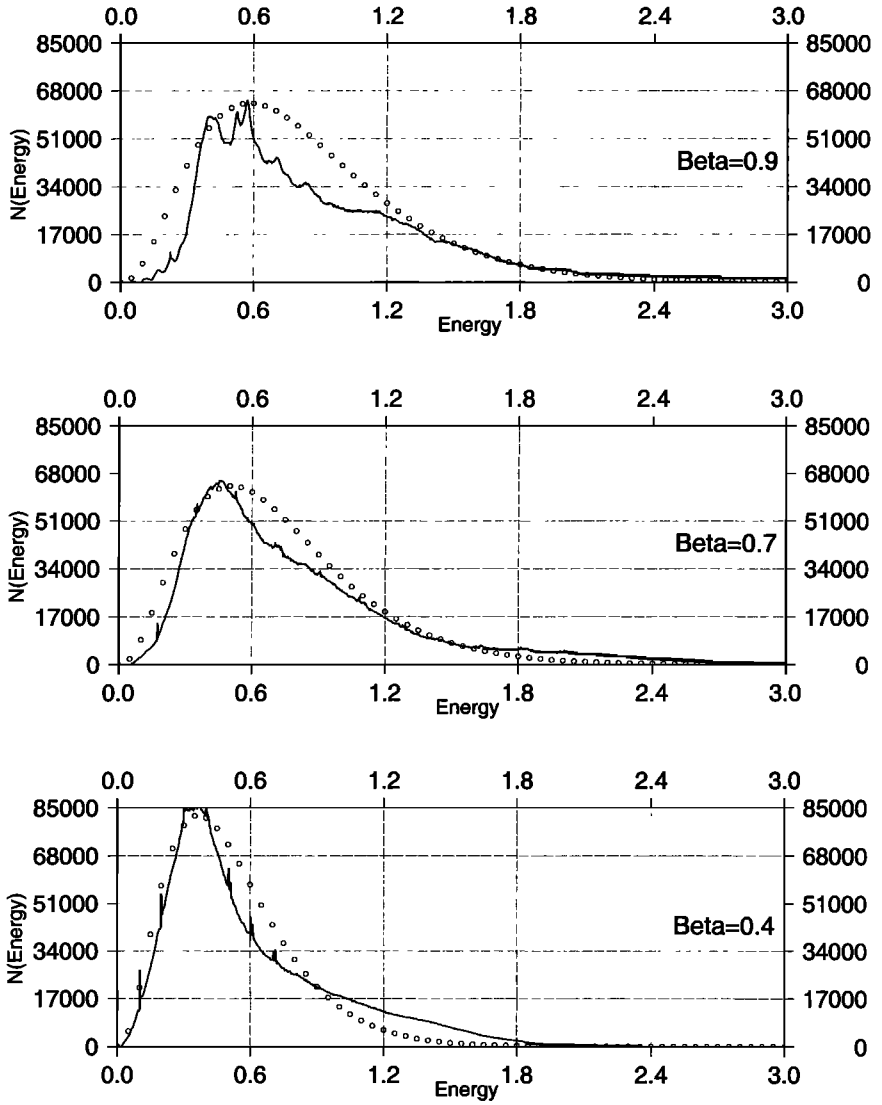

Figure 8. Plot of the energy distribution in the connecting springs, averaged over the whole model run, for different values of β. The diagrams also show the best fits to the data for equation (24) as circles.

trends can be seen in Figure 9 as β is increased. First, the mean energy averaged over the entire run increases. Second, the amplitude of the fluctuations also increases, most likely as a result of the large decoupling events which occur at and above the percolation threshold (β≥0.8). These large decoupling events represent a synchronicity in the dynamics despite the "thermal" disorder being added to the system, an example of "stochastic resonance" because of nonlinear feedbacks in the dynamics. This result is directly analogous to those of *Mousseau* [1996], who observed such synchronicity for low quenched disorder and for high conservation factors in the OFC model.

Finally, we examined the effect of varying absolute strength on the frequency-rupture area distribution, shown on Figure 11 for β=0.95, again averaged over 4000 time steps. The diagram shows that the form of the distribution is not strongly affected by the absolute fault strength, although the total number of events (intercepts on Figure 11) is systematically higher for weaker faults. Thus the absolute fault strength affects the event rate but not the *b* value or the correlation length.

4.2. Rough Fault

The elastic properties of the solid Earth are not in general homogeneous, so we also examined the case of spatially heterogeneous faults. We represent this heterogeneity in the form of uncorrelated noise chosen by a random-number generator. Although it is known that the material properties of natural rocks are spatially correlated (in fact, usually fractal), we assume an uncorrelated strength distribution illustrated in Figure 3b, so that the scale-invariant nature of the distributions (the power law part of (3)), if it exists, is truly emergent.

4.2.1. Statistical properties. We present and analyze the results in exactly the same manner as described above for smooth faults. The fault heterogeneity is described by the minimum and the maximum normalized strength. We first consider the case σ_F^{min}=0.5 and σ_F^{max}=1.5, so that the average

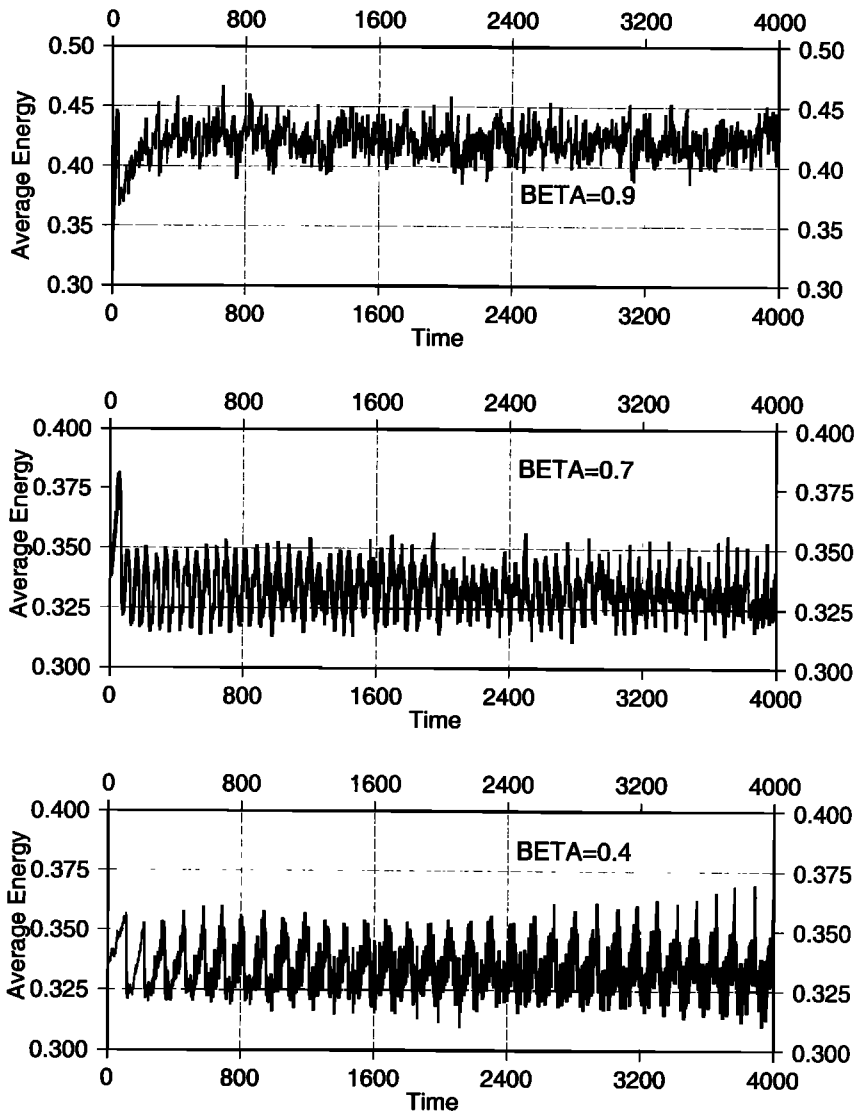

Figure 9. Plot of mean energy $\overline{E}$ for each time increment as a function of time increment for different values of β for the case of a smooth fault.

strength $<\sigma_F>=1$ is the same as for the first suite of cases of smooth faults in section 4.1. The frequency-rupture area statistics, averaged over the whole run, are shown in Figure 12, along with the best fit lines to (22), with parameters also summarized in Table 1. The effect of introducing heterogeneity acts to maintain a finite correlation length in all of these simulations, since $c>0$ for all values of β. Thus the heterogeneous material, even with the same average local strength, is globally much stronger than the homogeneous material. This result is consistent with the observation in material science that composite materials, even with the same local average strength, are stronger at a macroscopic scale because the stronger elements exert a disproportionate influence on the macroscopic strength. In this case the value of the exponent $\tau \approx 1$ stays relatively constant as β is increased, whereas c decreases systematically with respect to β, indicating an increase in correlation length. This is in contrast to the behavior in Figure 5 for a smooth fault, where the correlation length stays relatively constant and the power law exponent varies more strongly.

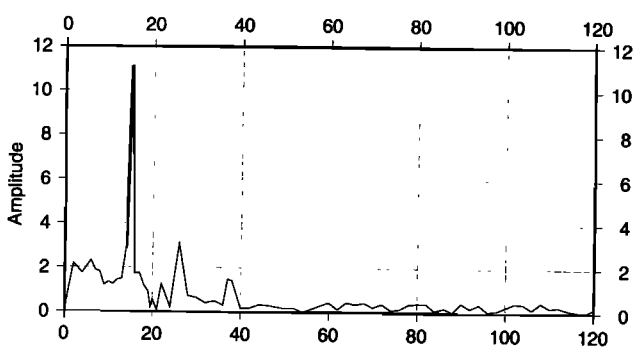

Figure 10. Spectrum of $\overline{E}$ (t) for the case β=0.6.

The energy distribution in the leaf springs is shown in Figure 13. In the heterogeneous case, all of the distributions show a Boltzmann exponential, and distinct energy quanta are absent. The energy distribution in the connecting springs

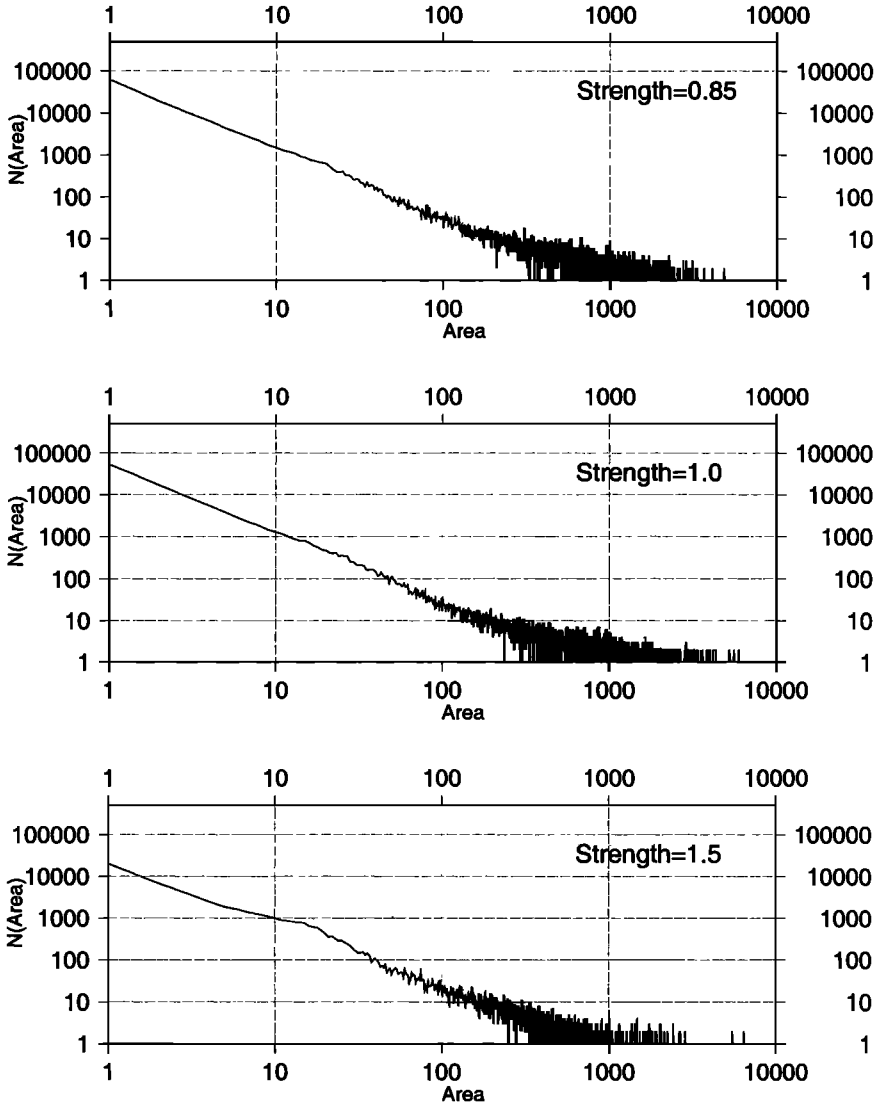

Figure 11. Frequency-rupture area distributions for different absolute fault strength for a smooth fault for the case β=0.95.

for the heterogeneous case is also consistent with the form of (24), as shown in Figure 14. In this case the parameter γ is more variable with respect to β than for the case of smooth faults, although it remains in the range 1.8-2.7, again systematically higher than the value of unity predicted for a system with 4 degrees of freedom, and furthermore implying a noninteger l. Here θ is systematically higher for the heterogeneous case, implying a higher mean energy $\overline{E}$. This is most likely a consequence of the absence of large-scale relaxation events.

Finally, we investigated the effect of increasing σ_F^{max}, as shown in Figure 15, for the case β =0.95. As σ_F^{max} is increased, the correlation length decreases, as inferred from the move to smaller rupture areas in the largest events, although the slope τ remains relatively constant. Thus heterogeneous faults are stronger, in the sense that they have smaller correlation lengths for connected broken elements. This implies, in turn, that they can hold more elastic strain energy that smooth faults, as observed above.

4.2.2. Energy fluctuations. Figure 16 shows the fluctuations in $\overline{E}(t)$ for the heterogeneous case. The same quasi-periodic fluctuations are seen for high local dissipation, with a mean recurrence period of t_R=3000/16=187, again shorter than t_C but longer than the equivalent recurrence time for the homogeneous example. Note that in this case the quasi-periodic oscillations decay with time. The mean energy level in these plots increases systematically with β, similar to that seen in the heterogeneous case. However, as the mean energy increases, the amplitude of the statistical fluctuations in $\overline{E}$ decreases, exactly the opposite of the case for smooth faults (compare Figures 9 and 16). The curve for β=0.9 on Figure 16 shows a nearly constant energy, implying efficient tuning to a stationary state, albeit with a finite correlation length, and hence the system remains below the critical point.

4.3. Comparison of Smooth and Rough Faults

In this section we compare the behavior of the two model classes by plotting the different model parameters for varying β. First, Figure 17 plots the mean energy $\overline{E}$, averaged over the whole run, which increases systematically for both

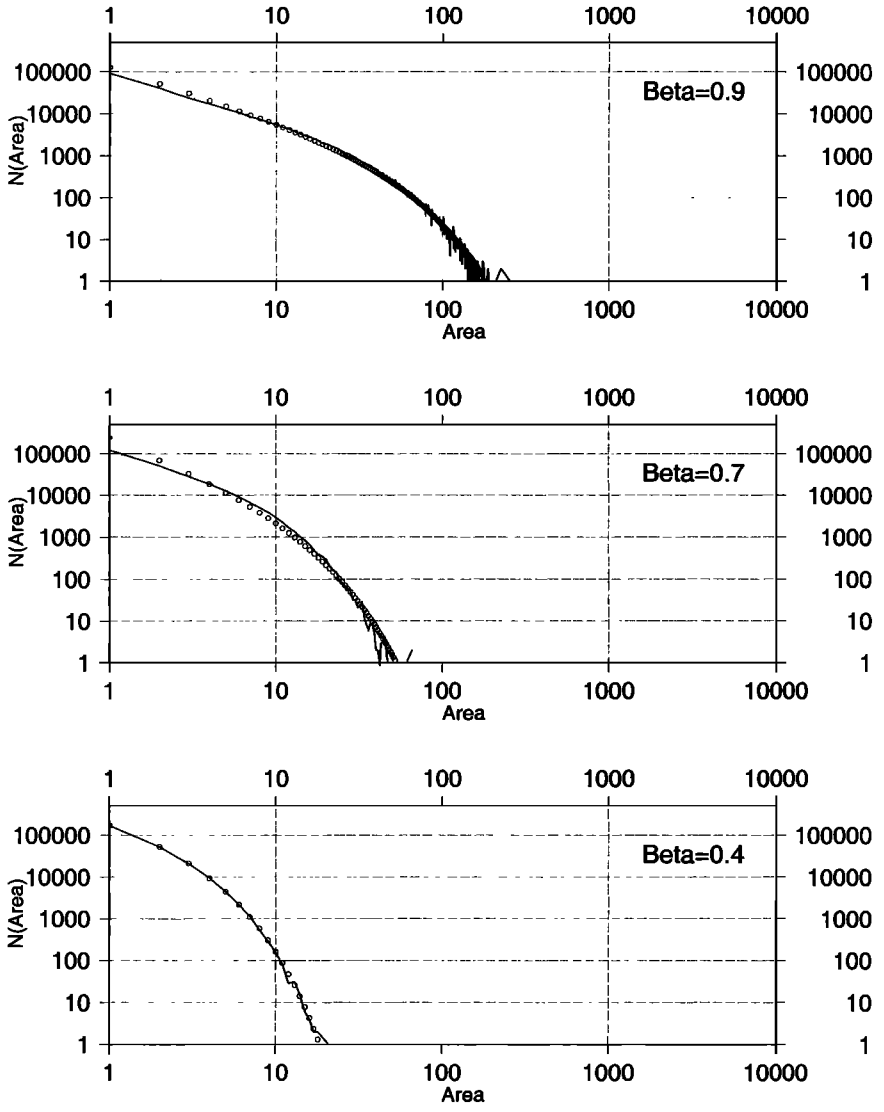

Figure 12. Frequency-rupture area statistics for a heterogeneous fault with a random strength distribution in the range 0.5-1.5 for different values of β.

models as β increases. The heterogeneous model produces systematically higher $\overline{E}$ in all cases, and the difference between the two increases systematically with increasing β. The predicted seismic *b* value, assuming $b=\tau$, shows a systematic decrease with respect to β in both cases (Figure 18). In all cases the homogeneous fault produces larger *b* values, the difference increasing systematically with increasing dissipation. This negative correlation of *b* value with β is similar to that seen in the model of *Olami et al.* [1992]. In contrast, the parameter *c*, which is related inversely to the correlation length, is systematically lower for the smooth model (Figure 19). The difference in *c* between the two models decreases as the dissipation factor increases. The combination of results in Figures 18 and 19 implies that the two models are reacting differently to changes in the local level of energy conservation. For the smooth model the correlation length is large and relatively fixed, so variations have to be accommodated by changes in *b* value. For the rough fault the correlation length is variable for all values of β studied here. The variable correlation length implies that the *b* value can remain relatively fixed, although a weaker negative correlation between *b* and β is still discernible in Figure 18.

4.4 Mean Energy and Tectonic "Temperature"

The mean energy is the first moment of the energy distribution. In the limit of large numbers of elements the summations in (12) are replaced by integrals

$$\overline{E} = \int_0^\infty Ef(E)dE \,/\, \int_0^\infty f(E)dE \qquad (25)$$

where $f(E)$is the probability density distribution of the form

$$f(E) \sim E^{\gamma-1} e^{-E/\theta}. \qquad (26)$$

For the case $\gamma \neq 1$ ($l \neq 2$) it is straightforward to show from (25) and (26), after a change of variables to $E' = \overline{E}/\theta$, that

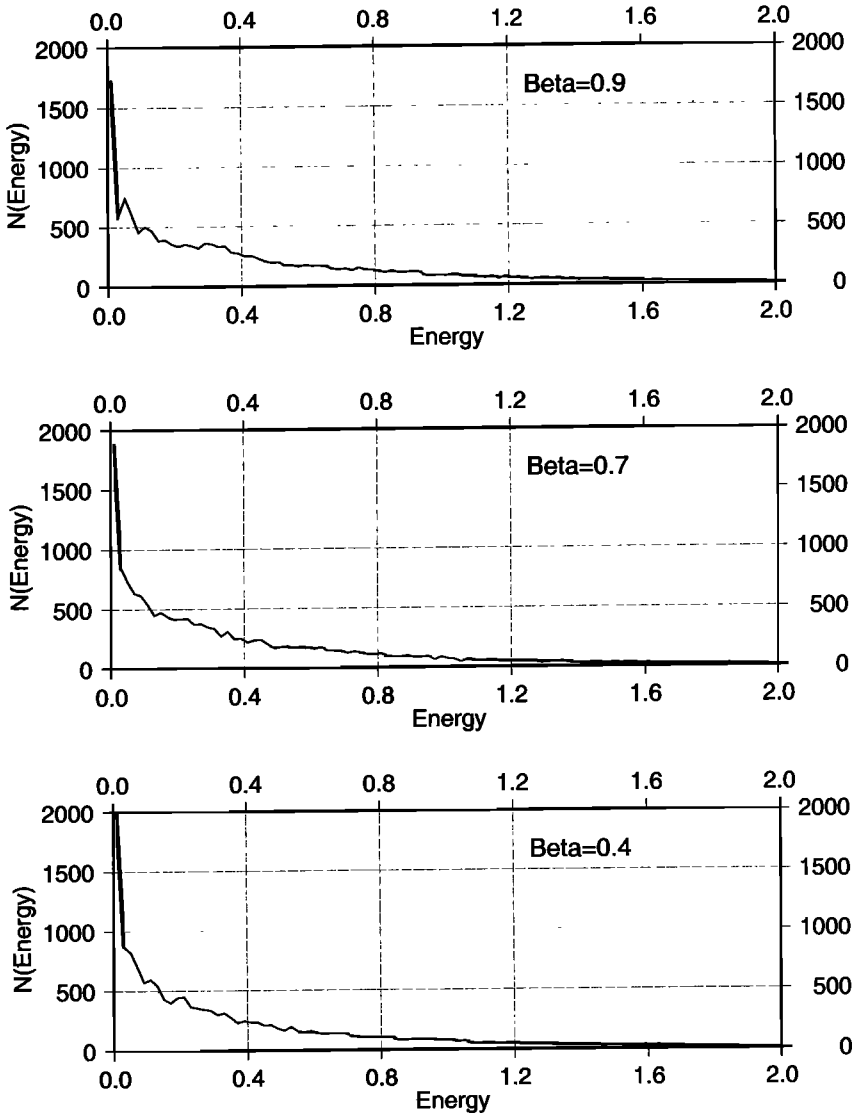

Figure 13. Energy distribution in the leaf springs, averaged over a model run for a heterogeneous fault with a random strength distribution in the range 0.5-1.5 for different values of β.

$$\overline{E} = \theta\,\Gamma(\gamma+1)/\Gamma(\gamma), \tag{27}$$

where Γ is the gamma function, defined for $\gamma>-1$. We use the property $\Gamma(r+1) = r\,\Gamma(r)$ to simplify to

$$\overline{E} = \gamma\,\theta. \tag{28}$$

For $\gamma=1$ ($l=2$) the energy distribution (26) reduces to a Boltzmann exponential with

$$\overline{E} = \theta. \tag{29}$$

By analogy with thermodynamic systems we can define a tectonic "temperature" by

$$T_T = \overline{E}\,/k_T = (\gamma / k_T)\,\theta. \tag{30}$$

Here k_T has the same dimensions but is not equivalent to Boltzmann's constant, since it applies to a macroscopic elemental block size Δx much bigger than atomic fluctuations in elastic energy. Figure 20 plots θ as a function of $\overline{E}$ to test the linearity of the proposed relationship for both fault models. In both cases, γ is relatively constant (Table 1), so we see an approximately linear trend as predicted by (28). The variations in the best fitting slope and intercept on Figure 20 reflect to some extent the small but systematic differences in the exponent γ between the two models. However, the main cause is likely to be the small misfit to the tail of the frequency-energy distribution in Figures 7 and 8. A closer fit to (28) might be obtained if energy-weighted frequency data were used, so that the integral of such data would be closer to the first moment of the energy distribution. A similar fit to moment-weighted frequency data has recently been advocated by *Main* [1995] and *Amelung and King* [1997] to achieve a better match to tectonic moment release rates for similar reasons.

4.5. Tectonic Temperature and Correlation Length

In this section we examine the possibility of a relationship between the underlying energy distribution, determined by θ,

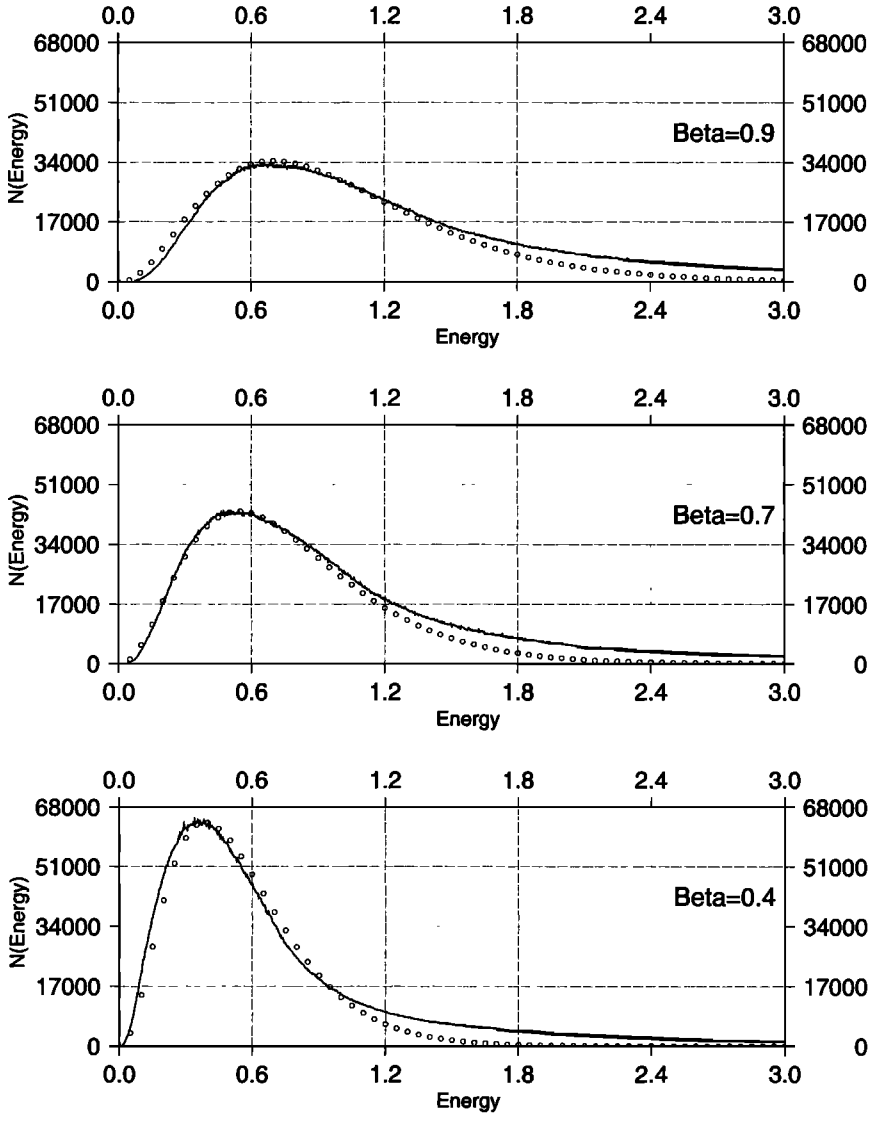

Figure 14. Energy distribution in the connecting springs, averaged over a model run for a heterogeneous fault with a random strength distribution in the range 0.5-1.5 for different values of β.

and the correlation length of the rupture area, related to S_o. Figure 21 shows a plot of $1/\theta$ against $1/S_o$ for the homogeneous and heterogeneous fault models. On Figure 21 we may consider positive S_o as defining the first phase and negative S_o as defining the second phase, analogous to the definition given by *Dahmen et al.* [1998]. Put simply, we may imagine the y axis on Figure 21 as the location of the analogous phase transition indicated in Figure 1. We note in both cases a strong positive correlation between θ and S_o, implying that the underlying distribution of strain energy as shown in Figure 6 is exerting a strong control on the resulting earthquake distribution (e.g., Figure 4). However, the slope on Figure 21 and the temperature at which the phase change takes place (i.e., the value of θ/k_T where $1/S_o=0$ or the intercept on the y axis) both depend on the material properties. In future work it will be important to examine this phase space in more detail by altering the model parameters over a wider range of possibilities than examined here.

5. Discussion

5.1. Self-Organized Criticality

None of the models above exhibit all of the strict features of self-organized criticality. For example, those which show an "infinite" correlation length (i.e., precisely critical behavior) show large rather than small fluctuations in the mean energy of the system (e.g., Figure 9 for β=0.9). In contrast, small fluctuations in E occur only in models which are subcritical in the sense of having a finite correlation length (Figure 16). In fact, few, if any, natural systems show all of the features required by an overly strict definition of self-organized criticality. This is not surprising, because the competition of fluctuations and interactions in any near-critical system is likely to result in an exploration of at least some of the phase space shown in Figure 1, and, in fact, the notion of self-organized criticality is invariably used in a broader sense to include such a range of behavior [*Bak*, 1997]. For the purposes of the work described here, a

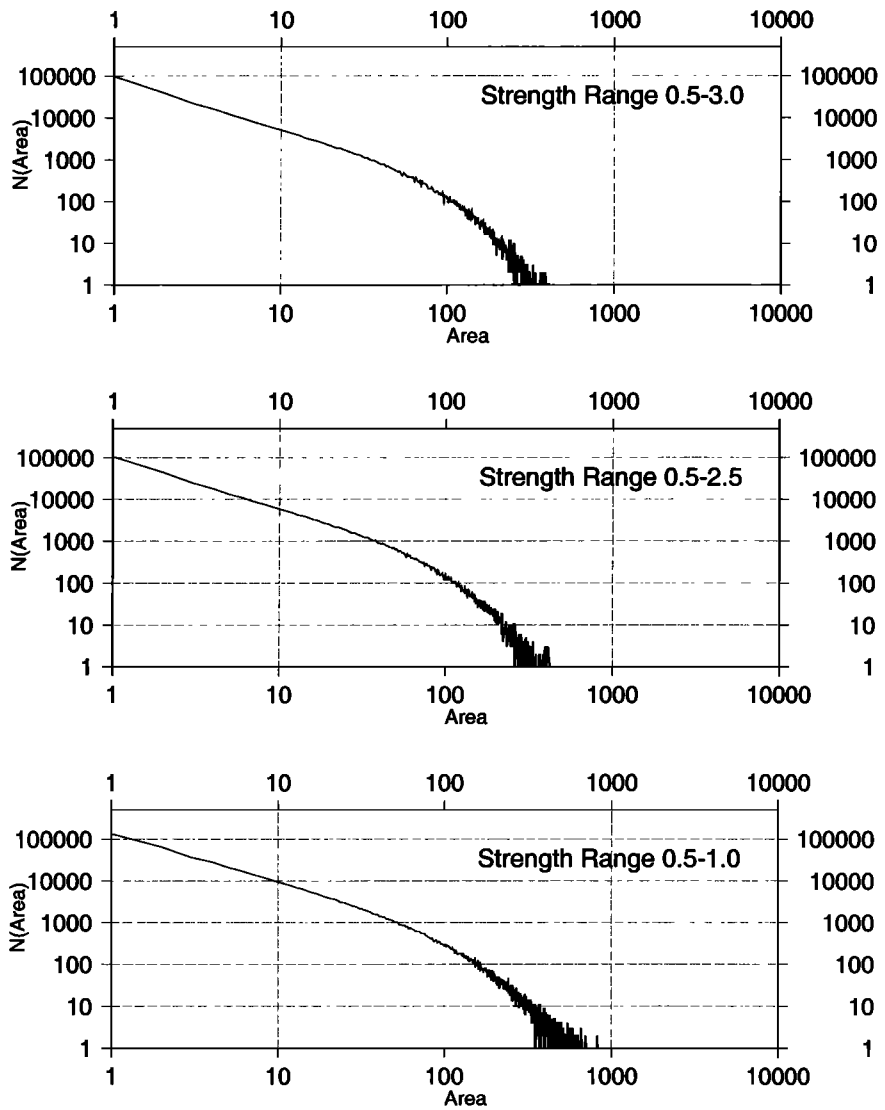

Figure 15. Frequency-rupture area statistics for a heterogeneous fault with a random strength distribution in the different strength ranges indicated for β=0.95.

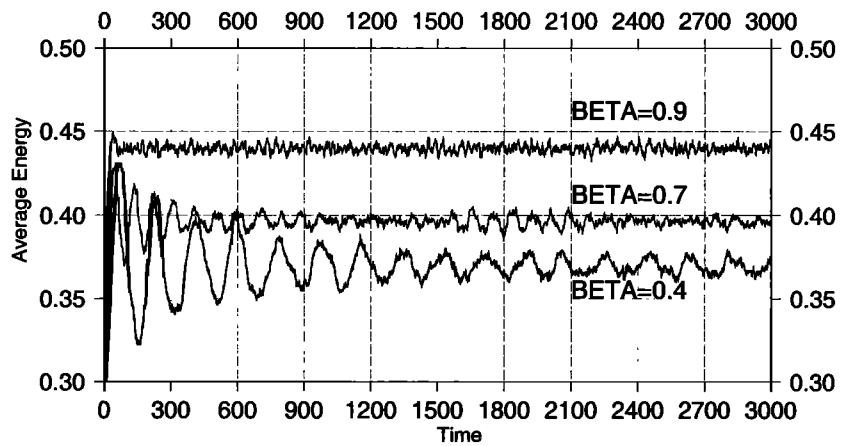

Figure 16. Plot of the temporal evolution of mean energy $\overline{E}$ for each time increment for different values of β for the case of a heterogeneous fault, with σ_F^{min}=0.5 and σ_F^{max}=1.5

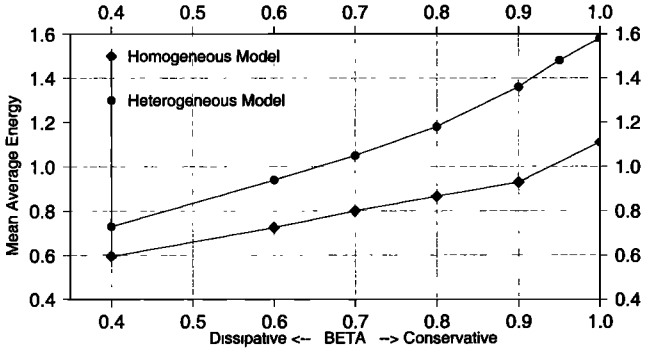

Figure 17. Plot of $\overline{E}$ averaged over the model run as a function of the conservation factor β for the "homogeneous" ($\sigma_F^{min}=\sigma_F^{max}=1$) and "heterogeneous" ($\sigma_F^{min}=0.5$ and $\sigma_F^{max}=1.5$) fault models.

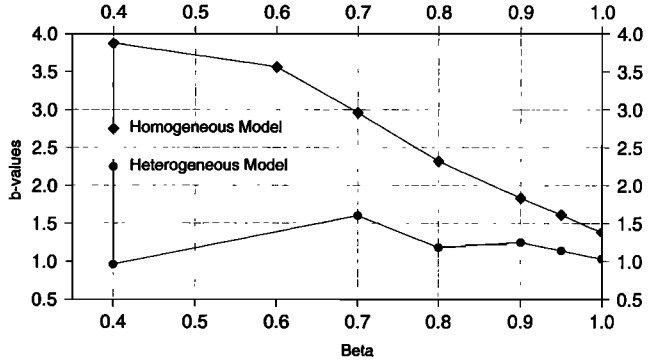

Figure 18. Plot of implied b value ($b=\tau$ assumed) as a function of the conservation factor β for the two models. "homogeneous" implies $\sigma_F^{min}=\sigma_F^{max}=1$; "heterogeneous" implies $\sigma_F^{min}=0.5$ and $\sigma_F^{max}=1.5$.

working definition is that the system should be maintained in a state which is sufficiently near critical that the power law scaling laws such as (3), (7), (8), and (9) all hold over some finite range. Finite fluctuations in energy are necessary in order to maintain the observed scaling rules but will maintain the system in a stationary state as long as they are small compared to the absolute energy of the system.

5.2 Model Simplifications

The model presented here assumes many simplifications which should be addressed in future work. First, we have examined the case of site percolation in a cellular automaton, that is, in the plane of a preexisting two-dimensional fault. However, the geological signature of an earthquake fault is usually in the form of a trace on a map, more analogous to a bond percolation problem [e.g., *Cowie et al.*, 1993]. In future work it will be important to examine any possible differences in the form of the scaling relations which might arise from this difference in geometry. Related to this, is the problem of a true three-dimensional representation of a fault population. The directionality of rupture implies that simple three-dimensional percolation may not be appropriate, unless it reflects the anisotropic nature of the stress field. Some anisotropic models for percolating networks have been developed, notably for applications in directed polymers, but these have so far not been applied to earthquake modeling.

The effect of long-range elastic interactions has been ignored in this work, but we have, nevertheless, seen that long-range correlations in the energy distribution can result from a propagation of short-range interactions. However, in future, it will be necessary to examine the effect of introducing the full elastic solution on the distributions and distribution parameters. Similarly, different forms of material heterogeneity, involving correlated elastic properties (both strengths and moduli) should be investigated in order to determine to what extent the observed correlations in the model output are conditioned by preexisting correlations in the quenched (time independent) disorder or arise as a consequence of the competition between fluctuations and interactions described in section 2.4 (time dependent disorder). In this context it should be noted here that some small-scale correlations may be present even in our "random" strength heterogeneity, because of the nature of the algorithms currently used to generate random numbers [*Stauffer and Aharony*, 1994].

5.3 Log-Periodic Fluctuations

The appearance of preferred energy states for high degrees of local energy conservation on smooth faults is another emergent property of the model for smooth faults with low dissipation. An energy spectrum with preferred (quasi-periodic) energy peaks is also a feature of the analytical

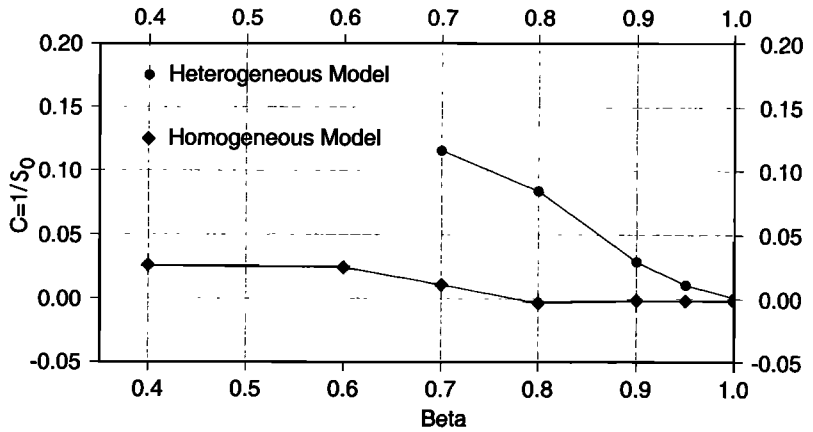

Figure 19. Plot of c for the two models as a function of the conservation factor β for the two models. "homogeneous" implies $\sigma_F^{min}=\sigma_F^{max}=1$; "heterogeneous" implies $\sigma_F^{min}=0.5$ and $\sigma_F^{max}=1.5$.

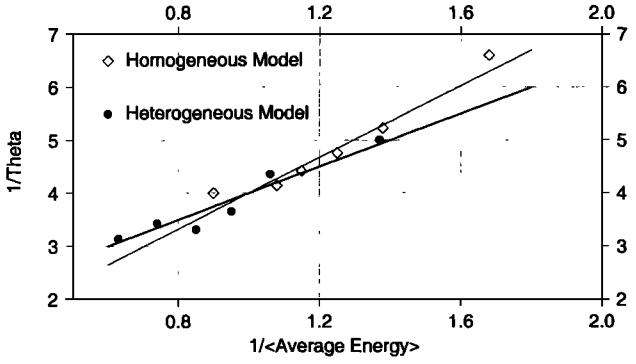

Figure 20. Plot of $1/\theta$ against $1/\overline{E}$ for the whole model run. The line fits assume the linear dependence implied for constant g_E by equation (28). "homogeneous" implies $\sigma_F^{min}=\sigma_F^{max}=1$; "heterogeneous" implies $\sigma_F^{min}=0.5$ and $\sigma_F^{max}=1.5$.

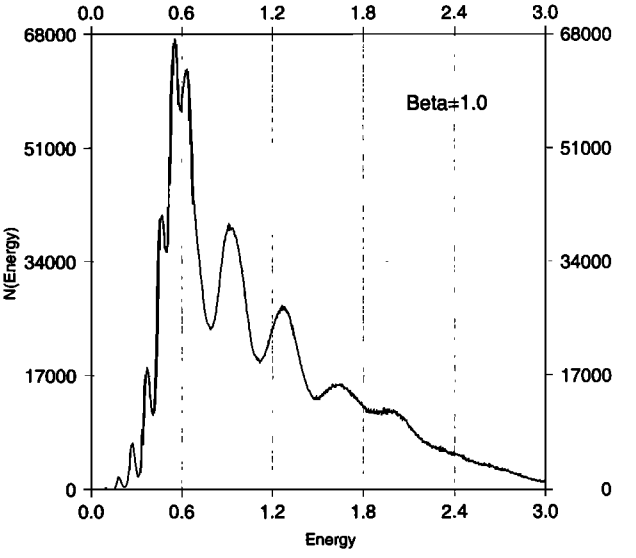

Figure 22. Plot of the energy distribution for $\beta=1$ for comparison with Figure 7.

random-neighbor version of the OFC model *by Chanabol and Hakim* [1997]. The preferred energy states in our numerical model take the form of log-periodic modulations on the overall trend, and the number of peaks varies with the energy conservation factor. For example, Figure 7 shows a systematic increase in the number of peaks in the energy distribution of the leaf springs with increasing β. This hierarchy of energy states is entirely absent in the heterogeneous models and results in longer-range spatial correlations at those energy values than would otherwise be the case (e.g., Figure 6). The connecting springs show well-developed, approximately log-periodic quanta for the case of a smooth fault with no local dissipation (Figure 22). These results are interesting because a hierarchical spatial structure has independently been suggested as a possible explanation for log-periodic modulations on the nonlinearly increasing Benioff strain, based on seismic energy release rates observed before some earthquakes [*Sornette and Sammis*, 1995; *Varnes and Bufe*, 1996; *Sornette*, 1998].

An accelerating strain rate before earthquakes is plausible on theoretical grounds because time appears as a scaling field in the traveling density wave model of *Rundle et al.* [1997a, b] and is a feature of the rheology of materials deforming by subcritical crack growth [*Bufe and Varnes*, 1993; *Main*, 1999]. However, in practice, the general existence of precursory accelerating strain has proved elusive to detect, either based on direct geodetic measurements at Earth's surface or inferred from a host of proposed associated precursors. For example, the null hypothesis of a time-independent (Poisson) model produces a better fit to global data sets of Benioff strain rate than one of accelerating strain in the study of *Gross and Rundle* [1998]. Thus the first-order observation of accelerating strain has yet to be established in a general sense before the second-order log-periodicity can be examined in detail. On theoretical grounds, log-periodic fluctuations are an approximation resulting from a second-order truncation of the more general parametric homogeneous functions described by *Borodich* [1994], so it is perhaps not surprising that their general existence is difficult to prove definitively.

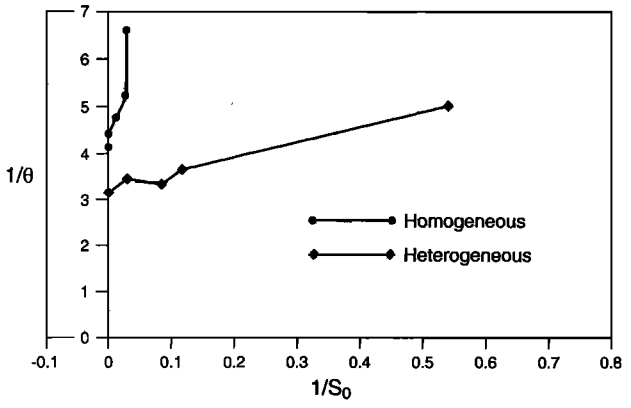

Figure 21. Plot of $1/\theta$ against $c=1/S_0$ for the "homogeneous" ($\sigma_F^{min}=\sigma_F^{max}=1$) and "heterogeneous" ($\sigma_F^{min}=0.5$ and $\sigma_F^{max}=1.5$) fault models.

The observation of discrete peaks in the energy distribution may reasonably be challenged on the grounds of the relatively short timescales applied in this paper ($\sim 10^4$ time steps). Accordingly, Figure 23 shows the energy distributions in the leaf springs for the smooth fault model, run over 10^6 time steps for $\beta>0.8$ In both examples the log-periodic fluctuations are retained, so this phenomenon is not a statistical transient over these timescales. The resulting fluctuations in mean energy as a function of time, shown in Figure 24, also exhibit a decrease in amplitude with increasing mean energy and a positive correlation of $\overline{E}$ with β, as observed in Figure 9.

On theoretical grounds, *Saleur et al.* [1996] developed a geometric model for log-periodic fluctuations based on a model brittle crust with a hierarchical structure determined by a complex fractal dimension. The model presented here is one example of how such log-periodic fluctuations in the energy distribution, related to a correlated hierarchy of structures, may be introduced spontaneously as a consequence of a particular set of dynamic conditions. Most other physical models concentrate on log periodicity in event (avalanche) sizes, for example, the power law modulated by log-periodic peaks in the version of the *Burridge-Knopoff* [1967] model proposed by *Elmer* [1997] and the discrete

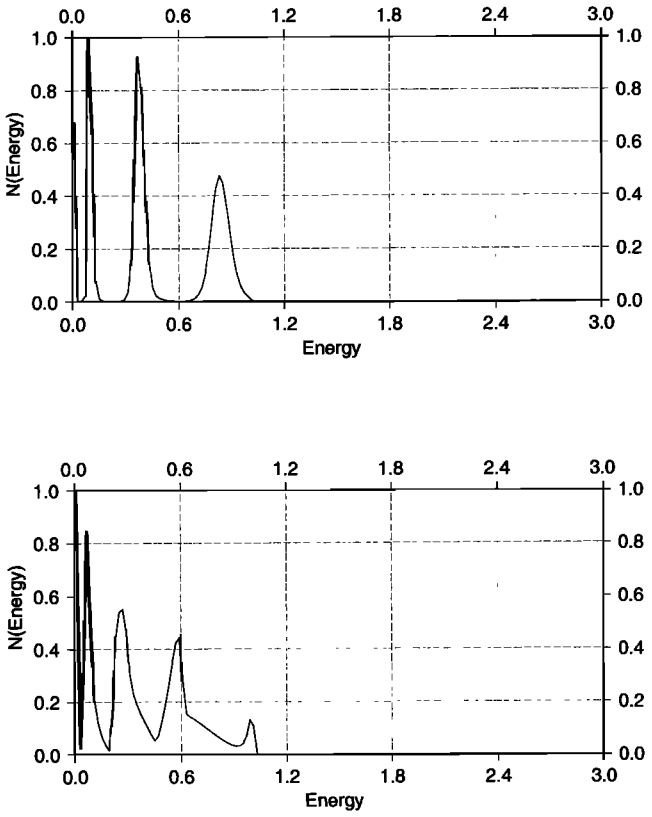

Figure 23. Plot of the normalized energy distribution for β=1 (upper diagram) and β =0.9 (lower diagram) in the leaf springs for two model runs on the homogeneous fault model over a time period of 10^6 increments.

hierarchy in sliding events observed by *Huang et al.* [1997]. Such models give a physical rather than a purely geometrical basis to the possibility of a log-periodic geometrical hierarchy of structure in Earth's brittle crust, but the true test of the utility of this observation will remain with more detailed observation of possible accelerating strain before earthquakes.

5.4. Heterogeneity and *b* Values

All of the model results for the heterogeneous material show $\tau \approx 1$ (Table 1). For seismometers acting as velocity transducers, we have seen that $b=\tau$, so the model b value is always around 1, consistent with this ubiquitous observation in natural seismicity data [*Turcotte*, 1992; *Main*, 1996]. For our model the resulting variability in the frequency-magnitude relation occurs predominantly because of variations in the correlation length, rather than the power law slope (Table 1). This feature of the model presented here is entirely consistent with *Kagan*'s [1997] observation of a relatively constant power law slope in natural seismicity data from the Harvard Centroid Moment Catalogue.

The results for the homogeneous strength model imply systematically higher values for b than for the heterogeneous model with the same characteristics otherwise. The results (Figure 18) therefore directly contradict the experimental observation [*Mogi*, 1967] that b values from acoustic emissions in laboratory tests tend to increase with increasing material heterogeneity. However, these (and other) experimental results were fitted solely with the two-parameter (1), often using data with a narrower bandwidth than possible with model simulations, and are hence not directly comparable with our three-parameter fits to (3) based on the predictions of percolation theory.

Whatever the cause for this difference, the results presented here suggest that a reexamination of acoustic emission data may be needed to see whether changes in b value or correlation length are, in fact, more strongly affected by material heterogeneity. Since an extra parameter is required to examine correlation length, any statistical model would have to include an appropriate penalty for the extra degree of freedom, as discussed for the case of the scaling of fracture opening displacement and length by *Main et al.* [1999]. In practice, it may be difficult to obtain a sufficient bandwidth of source rupture area to test this hypothesis definitively. In the meantime we should allow for the possibility that material heterogeneity exerts a strong control on the correlation length of seismic sources.

6. Conclusions

In this work we have tested the hypothesis that the output distributions of source rupture area and energy take the same form as those which might have been predicted from percolation theory or the statistical physics of critical point phenomena. We find that in all cases examined, the distributions do take the same form, although the parameters

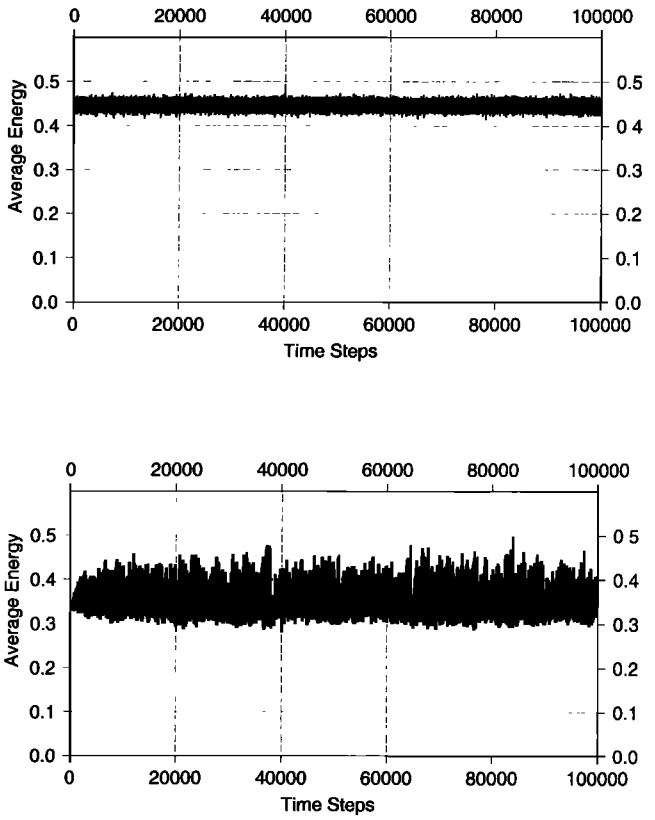

Figure 24. Plot of the mean energy for β=1 (upper diagram) and β =0.9 (lower diagram) as a function of time for the same model as in Figure 23.

vary systematically with the degree of heterogeneity and the strength of the local physical interactions, as measured by the local energy conservation factor β. In particular, both frequencies are distributed in the form of a gamma density distribution $n(S) \sim S^{\tau} \exp(-S/S_0)$ and $n(E) \sim E^{\nu} \exp(-E/\theta)$, respectively. The distribution parameters vary systematically with the controlling variables. The characteristic rupture area S_0, related to the correlation length, increases systematically with increasing material homogeneity and with increasing β, and θ is found to be proportional both to $\overline{E}$ and S_0. The latter implies that the underlying elastic potential energy distribution strongly affects the rupture size distribution. For heterogeneous faults, $\tau \sim 1$ stays relatively constant, and S_0 increases with increasing β or decreasing heterogeneity. In contrast, smooth faults produce a stronger decrease in τ with respect to β, and S_0 remains relatively constant. The scaling exponent ν varies systematically between the leaf springs and the connecting springs due to the difference in the number of available degrees of freedom. The output $\overline{E}(t)$ for both types of fault shows a transition from strongly quasi-periodic temporal fluctuations for strong dissipation to more chaotic fluctuations for more conservative models. Only strongly heterogeneous faults show the small fluctuations in $\overline{E}(t)$ strictly required by models of self-organized criticality, albeit with a finite correlation length implying subcritical behavior. Finally, for some conditions we observe log-periodic energy quanta which emerge spontaneously from the dynamics, rather than solely as a consequence of geometric renormalization constraints.

Acknowledgments. The first draft of this paper was prepared while I.G.M. was on sabbatical leave at the Department of Earth, Atmospheric, and Ocean Sciences at the Ecole Normale Superieure, Paris. He is grateful for their kind hospitality and for several stimulating discussions on the material contents of this paper, particularly with Yves Gueguen, Jean Schmittbuhl, Dmitri Pissarenko, Claude Froidevaux, and Teng-Fong Wong. We also appreciate the suggestions of two anonymous reviewers and Didier Sornette as Associate Editor, all of whose constructive comments significantly improved the presentation and context from an earlier draft.

References

Amelung, F., and G. King, Earthquake scaling laws for creeping and non-creeping faults, *Geophys. Res. Lett.*, *24*, 507-510, 1997.

Bak, P., *How Nature Works: The Science of Self-Organized Criticality*, Oxford Univ. Press, New York, 1997.

Bak, P., and C. Tang, Earthquakes as a self-organized critical phenomena, *J. Geophys. Res.*, *94*, 15,635-15,637, 1989.

Bak, P., C. Tang, and K. Wiesenfield, Self-organized criticality, *Phys. Rev. A, Gen. Phys.*, *38*, 364-374, 1987.

Ben-Zion, Y., J.R. Rice, and R. Dmowska, Interaction of the San Andreas fault creeping segment with adjacent great rupture zones and earthquake recurrence at Parkfield, *J. Geophys. Res.*, *98*, 2135-2144, 1993.

Borodich, F., Some applications of the fractal parametric-homogeneous functions, *Fractals*, *2*, 311-314, 1994.

Bruce, A., and D. Wallace, Critical point phenomena: Universal physics at large length scales, in *The New Physics*, edited by P. Davies, pp. 236-267, Cambridge Univ. Press, New York, 1989.

Bufe, C.G., and D.J. Varnes, Predictive modeling of the seismic cycle of the greater San Francisco Bay region, *J. Geophys. Res.*, *98*, 9871-9883, 1993.

Burridge, R., and L. Knopoff, Model and theoretical seismicity, *Bull. Seismol. Soc. Am.*, *57*, 341-371, 1967.

Carlson, J.M., and J.S. Langer, Properties of earthquakes generated by fault dynamics, *Phys. Rev. Lett.*, *22*, 2632-2635, 1989.

Ceva, H., Influence of defects in a coupled map lattice modeling earthquakes, *Phys. Rev. E, Stat. Phys. Plasmas Fluids Relat. Interdiscipl. Top.*, *52*, 154-158, 1995.

Chanabol, M.-L., and V. Hakim, Analysis of a dissipative model of self-organized criticality with random neighbours, *Phys. Rev. E, Stat. Phys. Plasmas Fluids Relat. Interdiscipl. Top.*, *56*, 2343-2346, 1997.

Christensen, K., Self-organization in models of sandpiles, earthquakes and flashing fireflies, *Ph.D. thesis*, Oslo Univ., Oslo, 1992.

Cowie, P.A., C. Vanneste, and D. Sornette, Statistical physics model for the spatio-temporal evolution of faults, *J. Geophys. Res.*, *98*, 21,809-21,821, 1993.

Dahmen, K., D. Ertas, and Y. Ben-Zion, Gutenberg-Richter and characteristic earthquake behavior in simple mean-field models of heterogeneous faults, *Phys. Rev E, Stat. Phys. Plasmas Fluids Relat. Interdiscipl. Top.*, *58*, 1494-1501, 1998.

Deiterich, J.H., Modeling of rock friction, 1: Experimental results and constitutive equations, *J. Geophys. Res.*, *84*, 2161-2168, 1979.

Elmer, F.-J., Self-organized criticality with complex scaling exponents in the train model, *Phys. Rev. E, Stat. Phys. Plasmas Fluids Relat. Interdiscipl. Top.*, *56*, 6225-6228, 1997.

Grassberger, P., Efficient large-scale simulations of a uniformly driven system, *Phys. Rev. E, Stat. Phys. Plasmas Fluids Relat. Interdiscipl. Top.*, *49*, 2436-2444, 1994.

Gross, S., and J. Rundle, A systematic test of time-to failure analysis, *Geophys. J. Int.*, *133*, 57-64, 1998.

Huang, G., H. Ouillon, H. Saleur, and D. Sornette, Spontaneous generation of discrete scale-invariance in growth models, *Phys. Rev. E, Stat. Phys. Plasmas Fluids Relat. Interdiscipl. Top.*, *55*, 6433-6447, 1997.

Ito, K., and M. Matsuzaki, Earthquakes as self-organized critical phenomena, *J. Geophys. Res.*, *95*, 6853-6860, 1990.

Janosi, I.M., and J. Keresz, Self-organized criticality with and without conservation, *Phys. A*, *200*, 179-188, 1993.

Kagan, Y.Y., Seismic moment distribution, *Geophys. J. Int.*, *106*, 123-134, 1991.

Kagan, Y.Y., Seismic moment distribution for shallow earthquakes: Regional comparison, *J. Geophys. Res.*, *102*, 2835-2852, 1997.

Leung, K.-T., J. Miller, and J.V. Andersen, Generalization of a two-dimensional Burridge-Knopoff model of earthquakes, *J. Phys. I*, *7*, 423-429, 1997.

Lomnitz-Adler, J., Automaton models of seismic fracture: Constraints imposed by the frequency-magnitude relation, *J. Geophys. Res.*, *98*, 17,745-17,756, 1993.

Main, I.G., Earthquakes as critical phenomena: Implications for probabilistic seismic hazard analysis, *Bull. Seismol. Soc. Am.*, *85*, 1299-1308, 1995.

Main, I., Statistical physics, seismogenesis, and seismic hazard, *Rev. Geophys.*, *34*, 433-462, 1996.

Main, I.G. Applicability of time to failure analysis to accelerated strain before earthquakes and volcanic eruptions, *Geophys. J. Int.*, *139*, F1-F6.

Main, I.G., T. Leonard, O. Papastiliotis, C.G. Hatton and P.G. Meredith, One slope or two? - Detecting statistically-significant breaks of slope in geophysical data, with application to fracture scaling relationships, *Geophys. Res. Lett.*, *26*, 2801-2804, 1999.

Mandl, F., *Statistical Physics*, 2nd ed., John Wiley, New York, 1988.

Middleton, A.A., and C. Tang, Self-organized criticality in non-conserved systems, *Phys. Rev. Lett.*, *74*, 742-745, 1995.

Mogi, K., Earthquakes and fractures, *Tectonophysics*, *5*, 35-55, 1967.

Mousseau, N., Synchronisation by disorder in coupled systems, *Phys. Rev. Lett.*, *77*, 968-971, 1996.

Olami, Z., H.J.S. Feder, and K. Christensen, Self-organized criticality in a continuous, non-conservative cellular automaton modeling earthquakes, *Phys. Rev. Lett.*, *68*, 1244-1247, 1992.

Rice, J. R., Spatio-temporal complexity of slip on a fault, *J. Geophys. Res.*, *98*, 9885-9907, 1993.

Romanowicz, B., Strike-slip earthquakes on quasi-vertical transcurrent faults: Implications for general scaling relations, *Geophys. Res. Lett.*, *19*, 481-484, 1992.

Rundle, J.B., W. Klein, S. Gross, and D. Turcotte, Boltzmann

fluctuations in numerical simulations of non-equilibrium threshold systems, *Phys. Rev Lett.*, *75*, 1658-1661, 1995.

Rundle, J.B., W. Klein, S. Gross, and C.D. Ferguson, Traveling density wave models for earthquakes and driven threshold systems, *Phys. Rev. E, Stat. Phys. Plasmas Fluids Relat. Interdiscipl. Top.*, *56*, 293-307, 1997a.

Rundle, J.B., S. Gross, W. Klein, C. Ferguson, and D.L. Turcotte, The statistical mechanics of earthquakes, *Tectonophysics*, *277*, 147-164, 1997b.

Saleur, H., C.G. Sammis, and D. Sornette, Discrete scale-invariance, complex fractal dimensions and log-periodic fluctuations in seismicity, *J. Geophys. Res.*, *101*, 17,661-17,677, 1996.

Schmittbuhl, J., J.-P. Vilotte, and S. Roux, A dissipation-based analysis of an earthquake fault model, *J. Geophys. Res.*, *101*, 27,741-27,764, 1996.

Scholz, C.H., A reappraisal of large earthquake scaling, *Bull. Seismol. Soc. Am.*, *72*, 1-14, 1994.

Sornette, D., Discrete scale-invariance and complex dimensions, *Phys. Rep.*, *297*, 239-270, 1998.

Sornette, D., and C.G. Sammis, Complex critical exponents from renormalization group theory of earthquakes: Implications for earthquake predictions, *J. Phys. I*, *5*, 607-619, 1995.

Sornette, D., and A. Sornette, Self-organized criticality and earthquakes, *Europhys. Lett.*, *9*, 197-202, 1989.

Sornette, D., P. Miltenberger, and C. Vanneste, Statistical physics of fault patterns self-organized by repeated earthquakes, *Pure Appl. Geophys.*, *142*, 491-527, 1994.

Stanley, H.E., *Introduction to Phase Transitions and Critical Point Phenomena*, Oxford Univ. Press, New York, 1971.

Stauffer, D., and A. Aharony, *Introduction to Percolation Theory*, 2nd *ed.*, Taylor and Francis, Philadelphia, Pa., 1994.

Turcotte, D.L., *Fractals and Chaos in Geology and Geophysics*, Cambridge Univ. Press, New York, 1992.

Varnes, D.J., and C.G. Bufe, The cyclic and fractal seismic events preceding an m_b 4.8 earthquake on 1980 February 14 near the Virgin Islands, *Geophys. J. Int.*, *124*, 149-158, 1996.

I.G. Main, Department of Geology and Geophysics, University of Edinburgh, West Mains Road, Edinburgh EH9 3JW, Scotland. Email: imain@glg.ed.ac.uk

G. O'Brien, University College Dublin, Belfield, Dublin 4, Ireland. Email: gareth.obrien@ucd.ie

J.R. Henderson, Elf Exploration UK PLC, 1 Claymore Drive, Aberdeen, AB23 8GB, Scotland. Email: jeremy.henderson@elfexp.co.uk

(Received February 24, 1999; revised October 19, 1999; accepted November 4, 1999.)